JACS
JOURNAL OF THE AMERICAN CHEMICAL SOCIETY
pubs.acs.org/JACS
Article

Z-Form Adoption of Nucleic Acid is a Multi-Step Process Which Proceeds through a Melted Intermediate

Parker J. Nichols, Jeffrey B. Krall, Morkos A. Henen, Robb Welty, Andrea Macfadden, Quentin Vicens,* and Beat Vögeli*

Cite This: J. Am. Chem. Soc. 2024, 146, 677−694
Read Online
ACCESS | Metrics & More | Article Recommendations | Supporting Information

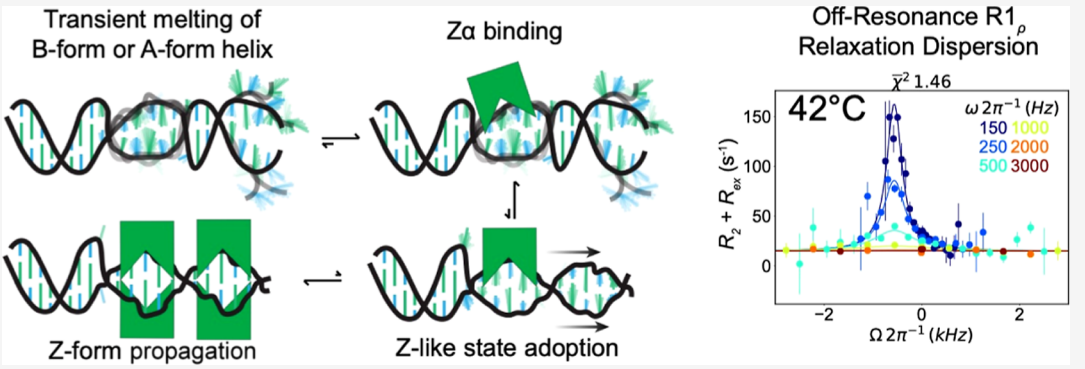

ABSTRACT: The left-handed Z-conformation of nucleic acids can be adopted by both DNA and RNA when bound by Zα domains found within a variety of innate immune response proteins. Zα domains stabilize this higher-energy conformation by making specific interactions with the unique geometry of Z-DNA/Z-RNA. However, the mechanism by which a right-handed helix contorts to become left-handed in the presence of proteins, including the intermediate steps involved, is poorly understood. Through a combination of nuclear magnetic resonance (NMR) and other biophysical measurements, we have determined that in the absence of Zα, under low salt conditions at room temperature, d(CpG) and r(CpG) constructs show no observable evidence of transient Z-conformations greater than 0.5% on either the intermediate or slow NMR time scales. At higher temperatures, we observed a transient unfolded intermediate. The ease of melting a nucleic acid duplex correlates with Z-form adoption rates in the presence of Zα. The largest contributing factor to the activation energies of Z-form adoption as calculated by Arrhenius plots is the ease of flipping the sugar pucker, as required for Z-DNA and Z-RNA. Together, these data validate the previously proposed "zipper model" for Z-form adoption in the presence of Zα. Overall, Z-conformations are more likely to be adopted by double-stranded DNA and RNA regions flanked by less stable regions and by RNAs experiencing torsional/mechanical stress.

INTRODUCTION

The most stable double-stranded helical conformations for DNA and RNA under physiological conditions are the B- and A-form, respectively. Both conformations are right-handed helices but otherwise differ in shape and geometry.[1] Nucleic acid binding proteins often exploit this fact in order to selectively recognize DNA or RNA.[2,3] Interestingly, both DNA and RNA will adopt a higher-energy, left-handed double-stranded conformation known as the Z-form under certain conditions (Figure 1A), such as when recognized and stabilized by Z-DNA/Z-RNA-binding Zα domains[4−8] or through chemical conditions/modifications (extensively reviewed here[9]). Other than the inverted helicity, the Z-conformation is more elongated compared to B-DNA/A-RNA and is composed of a repeating dinucleotide unit where the sugar puckers alternate between the C2′- and C3′-endo conformation along with the bases between the anti- and syn-conformations.[4,8−11] This arrangement leads to a lone pair−π contact only found within Z geometry (involving the O4′ of the C2′-endo sugar and the syn base[12,13]). The unique features of Z-form helices result in a jagged backbone conformation which "zig-zags" along the helical axis. This brings the phosphates closer together on average than in the B- or A-conformation, causing electrostatic repulsion and accounting for a significant contribution to the Z-form's intrinsic instability[14−18] (Figure 1A).

Received: September 24, 2023
Revised: December 4, 2023
Accepted: December 5, 2023
Published: December 22, 2023

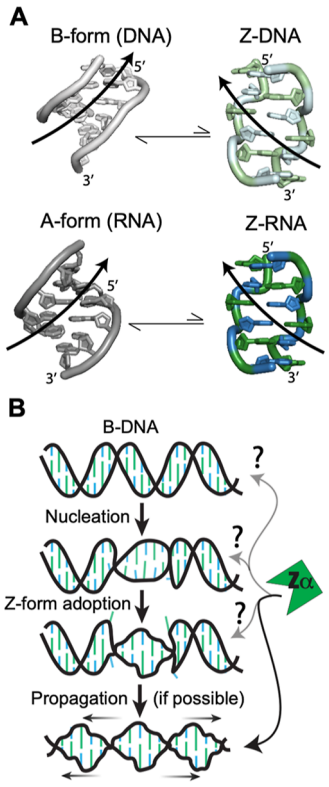

Figure 1. Characteristics of Z-DNA/RNA and Z-conformation adoption. (a) Both dsDNA (top) and dsRNA (bottom), normally in the B- and A-conformations, can adopt the higher-energy left-handed Z-form (right). Z-DNA and Z-RNA are structurally equivalent and will revert to the B/A-form in the absence of stabilizing factors. Pyrimidine (blue)−purine (green) repeats alternate between the C2′-endo and C3′-endo sugar pucker conformations along with the nucleobases between anti and the syn conformations. This leads to a zig-zagged backbone. B-DNA, A-RNA, Z-DNA, and Z-RNA models were made using PDBs 1N1K,[111] 1PBM,[112] 1QBJ,[5] and 2GXB,[6] respectively. (b) Zipper model for the conversion from B-DNA to Z-DNA.[31] First, a high-energy nucleation event allows for helical handedness conversion and a short Z-DNA stretch to be adopted. This can then propagate down the helix in a cooperative manner if the sequence allows it. At what point Zα plays a role in the zipper model is mostly unknown.

Despite these striking conformational changes, the Z-conformation retains Watson−Crick base-pairing.[8] Therefore, switching from the B/A-form to the Z-conformation requires both a 180° rotation of every nucleotide base in the helix about the glycosidic bond and a complete inversion of every other nucleotide (including the ribose), converting back to the anti-conformation.[19] This process is both topologically and thermodynamically challenging.[20] Over the years, different models have been proposed to theoretically address how this could occur.[8,19,21−30] The zipper model,[31,32] where an initial high-energy nucleation event allows a short Z-form segment enclosed between two B-Z junctions to be adopted, which then propagates through the helix in a cooperative manner, seems to fit the experimental evidence involving Z-DNA adoption well,[21,33] and is supported by molecular dynamics simulations[34] (Figure 1B).

Zα domains are found within a variety of innate immune response proteins or viral proteins and have been demonstrated to play pivotal roles in these proteins' ability to regulate the innate immune response or evade it, respectively.[35] These domains stabilize the Z-conformation of DNA and RNA by making key contacts with the unusual features present in Z-form helices.[6,36] Zα domains help to alleviate the steric repulsion of the closely placed, negatively charged phosphates by making charge−charge and water-mediated contacts with the Z-form backbone.[6,36] Previous Zα:nucleic acid structures have identified a number of key residues in the recognition and stabilization of the Z-conformation. Lys 169[5,6] and Asn 173[37] make contacts with the phosphate backbone. Pro 192 and Pro 193 position the beta-hairpin loop in a way which facilitates further interactions with the kinked Z-RNA backbone.[37] Trp 195 forms part of the hydrophobic core in addition to making a water-mediated contact with the phosphate backbone.[6,38,39] Tyr 177 is one of the most important residues, which makes a CH−π interaction with a syn base in the Z-form helix and is necessary for Zα to stabilize the Z-conformation[40,41] (Figure S1). The increasing number of discoveries of proteins containing functional Zα domains suggests that Z-conformations are being adopted in cells and play important biological function. However, what sequences and under what conditions these conformations are being adopted are still mostly unknown.[35]

Understanding the steps by which Zα domains stabilize Z-conformations in DNA and RNA is crucial to being able to predict the ability of varying sequence contexts to adopt the Z-form. Previous nuclear magnetic resonance (NMR) and Single-Molecule Förster Resonance Energy Transfer (smFRET) studies on Z-form adoption in the presence of Zα have shown the presence of multiple intermediate states between binding and Z-DNA/RNA adoption.[42−47] However, the identities of these states remain poorly understood (Figure 1B). One smFRET study showed that Zα bound to a presampled Z-conformation in a DNA duplex containing 5-methyl dCs (which lowers the energy barrier of Z-form adoption[48]), with the authors proposing that Zα recognizes a presampled Z-form state.[49] This is also supported by the fact that the Zα binding interface is preorganized to recognize Z-DNA/Z-RNA.[50] However, we still do not have a clear picture of how Z-forms are adopted and what role(s) Zα plays in the conversion. A better understanding of the Z-form adoption process via stabilization by Zα and the intermediate states involved would significantly improve our understanding of Z-form biology.

To help answer this question, we measured Off-Resonance $R1_\rho$ relaxation dispersion experiments[51] on model Z-forming d(CpG) and r(CpG) constructs. This experiment aims to probe for low population, dynamic states (in the μs-ms time scale) under low salt conditions and in the absence of Zα. The Off-Resonance $R1_\rho$ relaxation dispersion experiment allows for the characterization of microsecond-to-millisecond chemical exchange processes in solution,[52,53] a time scale which usually coincides with adoption of excited states.[54] These motions can lead to formation of "excited states" that correspond to local minima in the free energy landscape.[55] Our experiments revealed evidence of transient duplex melting, suggesting that helix melting may play a role in Z-form adoption. To study this further, we then carried out circular dichroism time-courses and other biophysical measurements to investigate the energy barriers of Z-form adoption in the presence of the Zα domain from human ADAR1,[56] one of the most well-characterized Zα domains.[5,6,36,57] We find that the ease of melting a duplex heavily correlates with its Z-form adoption rate and that the sugar pucker and nucleobase rearrangement are the rate-

https://doi.org/10.1021/jacs.3c10406
J. Am. Chem. Soc. 2024, 146, 677−694

limiting step for Z-form adoption. Finally, we find that duplex RNA goes through a single-stranded intermediate before Z-form conversion and that Zα's presence promotes the adoption of this single-stranded state. We speculate that while transient duplex melting is likely relatively frequent, transient Z-conformation likely only becomes populated when Zα is already bound to B/A-DNA/RNA and is, therefore, present to stabilize it. Consequently, we would predict that Z-conformations in the cell are quite stable, as they are either already in Z-form via stabilization by Zα domains or due to other mechanisms (such as helical torsion or chemical modifications).

RESULTS

Evaluating the Z-Form Stability of Model Z-Adopting d(CpG) and r(CpG) Constructs. To gain a better understanding of the Z-form adoption process and the intermediate states involved, we first looked for the existence of transient states in d(CpG) and r(CpG) sequences, which are well characterized Z-adopting sequences,[6,8,10,58,59] under low salt conditions (25 mM NaCl) where the Z-form would not be expected to form (Figure 2A). We chose these constructs because they each have a different energy barrier for adopting the Z-conformation and, theoretically, should have different populations of transient Z-conformations. Because the riboses in Z-form helices alternate between the C2′-endo and C3′-endo conformations, the 2′ hydroxyl in RNA represents a significant energy barrier to Z-form adoption.[60−62] We quantified Z-form adoption using circular dichroism titrations, which showed that in comparison to Z-DNA, Z-RNA needs more than double the salt concentration to be stabilized (4 and 5 M $NaClO_4$ for $r(CpG)_3$ and $r(CpG)_6$ constructs, respectively, compared to 2 M $NaClO_4$ for both the $d(CpG)_3$ and $d(CpG)_6$, Figures 2B, S2 and Table 1). The 5-methyl cytosine modifications in the $d(5mCpG)_3$ construct destabilizes the B-conformation relative to the Z-form, thereby significantly decreasing the energy barrier for Z-DNA adoption.[21,63−67] Its Z-form $NaClO_4$ midpoint is 800 mM which is 2.5x lower than the $d(CpG)_3$ construct (Figure 2B, Table 1). The 8-methyl guanine modification destabilizes both the B- and A-conformations of DNA and RNA by sterically clashing with the ribose when the base is in anti, resulting in the methylated purine adopting the syn conformation and thereby significantly promoting Z-form adoption.[68−70] Achieving Z-form midpoints for the 8mG4 $d(CpG)_3$ and 8mG4 $r(CpG)_3$ (8-methyl guanine at position 4) constructs requires 500× and 250× less $NaClO_4$ compared to the $d(CpG)_3$ and $r(CpG)_3$, with values of ∼4 and ∼16 mM, respectively (Figure 2B, Table 1). We also measured the melting temperatures (T_M) of the duplexes to make sure that they were in good agreement with predicted T_M values (Figure S3, Table 1). Overall, this data confirms that our selected constructs have different energy barriers for Z-form adoption and, therefore, are good candidates to probe for transient Z-conformations.

Off-Resonance $R1_\rho$ Relaxation Dispersion Measurements Reveal an Excited State in Model Z-Adopting d(CpG) and r(CpG) Constructs at 42 °C. We sought to probe for dynamic states during the A/B to Z transition. To this end, we recorded and assigned Off-Resonance $^{13}C-R1_\rho$[51] spectra of the $d(CpG)_3$, $d(5mCpG)_3$, 8mG4 $d(CpG)_3$, $r(CpG)_3$, and $r(CpG)_6$ constructs. In addition, we also measured ZZ-exchange experiments (which probe dynamics in the second time scale[71]) on the 8mG4 $d(CpG)_3$ and 8mG4 $r(CpG)_3$ constructs which are in slow exchange between the A/B and the Z-conformation and, therefore, served as positive controls. The presence of an excited state can be identified in the $R_2 + R_{ex}$ profile of the Off-Resonance $R1_\rho$ experiment by increased relaxation due to exchange at the excited state's chemical shift position (relative to the ground state). As the power of the ^{13}C spin-locking pulse is increased, the contribution of relaxation due to exchange is quenched, allowing for the exchange rate (k_{EX}) and difference in chemical shift ($\Delta\omega$) between the ground and excited states, as well as their populations (p_A and p_B), to be extracted (a theoretical illustration is shown in Figure S4A,C). ZZ-exchange allows characterization of slow time scale exchange processes by observing the transfer of longitudinal relaxation between the ground and excited states during mixing time, allowing for a direct readout of the exchange rate between the two states[72] (Figure S4B).

The $^{13}C-^{1}H$ HSQC and $^{1}H-^{1}H$ NOESY assignments and NOESY "walk" strategy for the assignment of B- and A-form

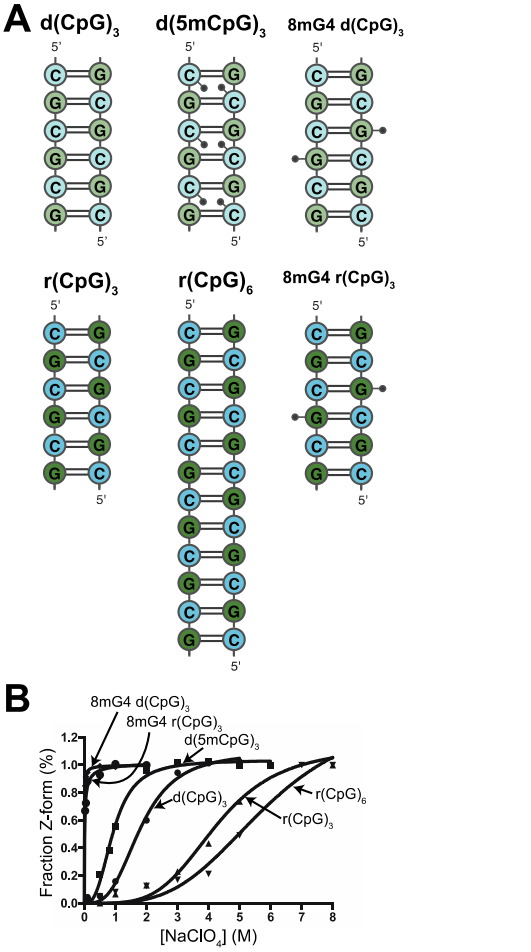

Figure 2. DNA and RNA constructs selected for NMR measurements. (a) 2D representations of the different d(CpG) and r(CpG) constructs used for NMR measurements in this study. DNA bases are more lightly shaded than RNA ones. Methyl groups for the modified constructs are depicted as small gray circles and indicate their relative position within the duplex. (b) Fits of circular dichroism titrations of $NaClO_4$ into the DNA and RNA constructs shown in (a), with the fraction of the duplex in the Z-conformation on the *y*-axis and the concentration of $NaClO_4$ (M) on the *x*-axis. The fraction of Z-DNA and Z-RNA was tracked by following the ellipticity at 264 and 285 nm, respectively, as described in the Methods sections.

https://doi.org/10.1021/jacs.3c10406
J. Am. Chem. Soc. 2024, 146, 677−694

Table 1. Duplex Constructs' Melting Temperatures and $NaClO_4$ Z-Form Midpoints Measured from Circular Dichroism[a]

construct	T_M (°C)	Z-form midpoint (M [$NaClO_4$])
$d(CpG)_3$	50.24 ± 0.00	1.923 ± 0.121
$d(5mCpG)_3$	54.04 ± 0.24	0.824 ± 0.093
8mG4 $d(CpG)_3$	26.01 ± 0.22	0.0044 ± 0.0005
8mG4 $d(CpG)_3$ (4:1 Zα:RNA)	59.80 ± 0.27	
$d(CpG)_6$	77.77 ± 0.74	1.867 ± 0.111
$d(CpG)_3TG(CpG)_2$	80.78 ± 2.59	1.683 ± 0.052
$(dCprG)_6$	55.41 ± 0.14	1.064 ± 0.157
$d(CpG)_{12}$	>100	1.770 ± 0.066
$r(CpG)_3$	49.22 ± 2.13	4.105 ± 0.162
8mG4 $r(CpG)_3$	A-form: 49.49 ± 5.38 Z-form: 22.76 ± 0.60	0.0164 ± 0.0066
8mG4 $r(CpG)_3$ (4:1 Zα:RNA)	64.32 ± 0.32	
$r(CpG)_6$	86.36 ± 0.86	5.218 ± 0.185
$r(CpG)_3UG(CpG)_2$	54.02 ± 4.09	6.299 ± 0.207
$r(CpG)_2CIUG(CpG)_2$	38.39 ± 0.46	5.013 ± 0.222
$r(CpG)_{12}$	>100	5.513 ± 0.119
$(dCpLG)_6$	N/A	N/A
$r(CpG)_3$ cUUCGg tetraloop	N/A	>6
$r(CpG)_3$ 6mer Ura loop	77.72 ± 1.82	>6

[a]N/A means that the melting temperature could not be measured over the range measured.

helices are shown for $d(CpG)_3$ (Figure 3A,B, Table S1). Assignments for the other constructs are shown in Figures S5−S12, and chemical shift values can be found in Tables S2−S6. We note that due to the palindromic nature of all the constructs we tested, the two strands are chemically equivalent (Figure 3A,B). For example, the aromatic CH8 peak of G4 is actually two overlapped peaks with identical chemical shifts, one from G4 of one strand and the other from the second strand. Therefore, all NMR observables for these constructs represent the average of the residue in question from both strands.

For the $d(CpG)_3$ construct at 25 °C in 25 mM NaCl, we obverse no μs-ms time scale exchange processes in our Off-Resonance $R1_\rho$ profiles that can be fit with any reasonable confidence (Figure 4, dispersion profiles for other residues are shown in Figure S13). This indicates that at 25 °C, either the $d(CpG)_3$ is not in exchange with a transient state on this time scale or that the excited state's population and dynamics is beyond detection by our experimental procedure (<0.5−1% population).

Because Z-form adoption is an entropically driven process and known to be promoted as a function of temperature,[36] we measured the same experiment at 42 °C (a commonly used incubation temperature with Zα[36]). The hypothesis we tested was that the increased temperature may promote the population of any transient Z-form state. At 42 °C, a clear excited state is populated for all residues of the $d(CpG)_3$ construct except for cytosine 1 and guanine 6 (Figures 4 and S13). Due to the similarity of the extracted exchange parameters for all residues, we fit them globally, which gave an exchange rate (k_{EX}) of 1630 ± 140 s^{-1} and an excited state population (p_B) of 4.0 ± 0.6% (Table 2). In addition, the excited state chemical shift differences ($\Delta\omega$) for all residues were downfield (deshielded) relative to their ground-state positions (Table 2), suggesting that the entire $d(CpG)_3$ construct was experiencing the same exchange process and that this excited state resulted in a more open conformation of the duplex, as would be predicted for the aromatic purine C8 atoms of Z-conformation (Figure S14).

We observed a similar phenomenon for the $d(5mCpG)_3$ and $r(CpG)_3$ constructs, with no observable exchange processes at 25 °C but a clear excited state at 42 °C (Figures 4, S15 and S16, Table 2). Again, we were able to fit the data from both constructs globally, which gave an exchange rate of 1300 ± 280 s^{-1} with a population of 2.0 ± 0.5% for the $d(5mCpG)_3$ construct and an exchange rate of 977 ± 53 s^{-1} with a population of 1.93 ± 0.06% for the $r(CpG)_3$ construct (Table 2). To test the stability of the fits, we also fixed k_{EX} over a range of values while fitting the population and chemical shift differences. For the $r(CpG)_3$ construct, there is a steep increase in χ^2, whereas it is flatter for the $d(CpG)_3$ and $d(5mCpG)_3$ constructs, where a less than 10% increase is compatible with k_{EX} deviations of ∼1000 and ∼3000 s^{-1}, respectively. When fixing k_{EX} over these ranges of values, the population and chemical shift differences vary little for the $r(CpG)_3$ construct, while they show some moderate variation for the $d(CpG)_3$ and $d(5mCpG)_3$ constructs (Figure S17A−C, Table S7). Similar to the $d(CpG)_3$ case, the excited state chemical shift differences for the fit residues in the $d(5mCpG)_3$ and $r(CpG)_3$ constructs displayed downfield chemical shift values. In contrast, the $r(CpG)_6$ duplex has no observable exchange process at 42 °C (Figures 4 and S18). This suggests that all three of the 6 bp constructs are sampling a similar state with different dynamics. However, the identity of this state is unknown without comparing its chemical shift difference ($\Delta\omega$) to what would be expected between the B/A- and Z-forms.

Excited State Chemical Shifts from Off-Resonance $R1_\rho$ Correlate with Melted Duplex Better than with Stabilized Z-DNA/Z-RNA. To identify whether the excited states observed at 42 °C in the $d(CpG)_3$, $d(5mCpG)_3$, and $r(CpG)_3$ constructs were a transient Z-conformation or other exchanging states, we needed to determine the chemical shift difference between the aromatic residues in the B-form/A-form and in the Z-form for the DNA and RNA constructs. To this end, we assigned the ^{13}C, ^{1}H chemical shifts of the 8mG4 $d(CpG)_3$ and 8mG4 $r(CpG)_3$ constructs, the DNA version of which had been previously confirmed to be in slow exchange between the B- and Z-conformations.[68] To our knowledge, the Z-forming capability of the singly methylated 8mG4 $r(CpG)_3$ has not been tested until now, although the construct is chemically similar to the double-methylated m8Gm (8-methyl and 2′-*O*-methyl guanosine) $r(CpG)_3$ construct which has been studied previously.[69]

Assignment and peak analysis of the HSQC spectrum recorded on the 8mG4 $d(CpG)_3$ construct (Figures S6 and S7) confirmed that the construct is indeed in a slow exchange between the B- and Z-conformations (Figure 5A) being mostly Z-form with a B-form population of 8.3 ± 2.3% at 25 °C (as determined from peak volume integration, Table 3). The extracted excited state chemical shift differences from the Off-Resonance $R1_\rho$ experiments measured on the $d(CpG)_3$ at 42 °C exhibit a high degree of correlation with the chemical shift difference between the B- and Z-form peaks in ^{13}C, ^{1}H HSQC of the 8mG4 $d(CpG)_3$ construct (Figure 5B, R^2 = 0.89). However, in all cases except for Cyt5 C6, they agree much

https://doi.org/10.1021/jacs.3c10406
J. Am. Chem. Soc. 2024, 146, 677−694

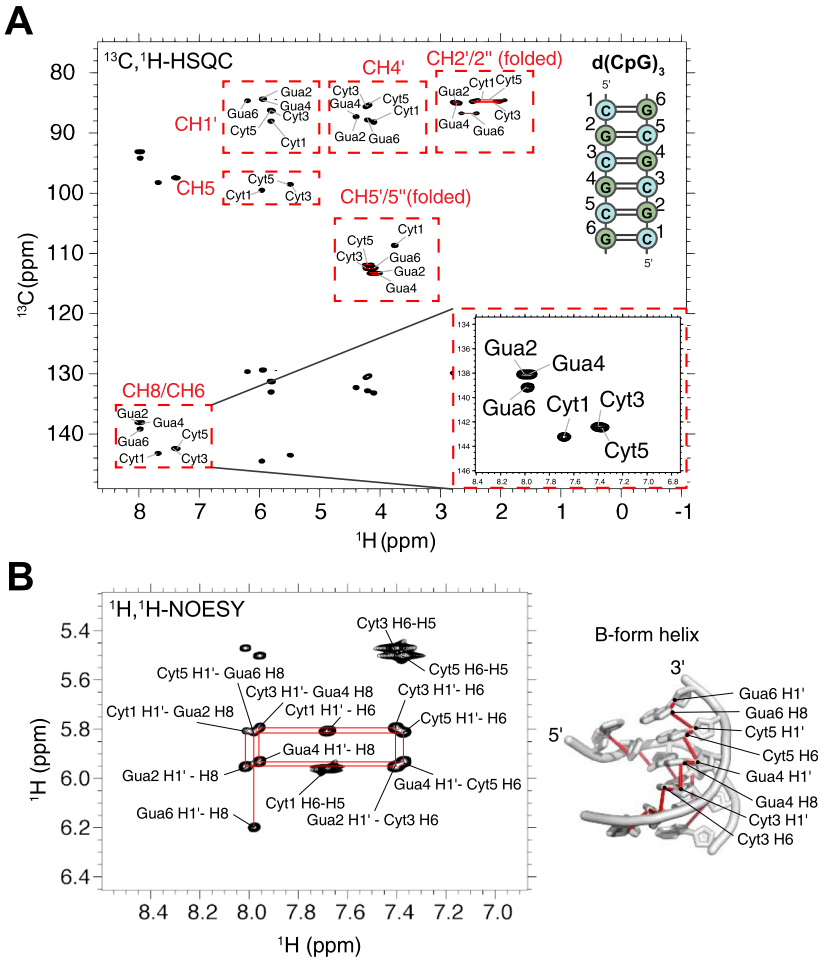

Figure 3. NMR assignment of the d(CpG)$_3$ construct. (a) Full ^{13}C−^{1}H HSQC spectra assignments for the d(CpG)$_3$ construct are shown (depicted on the right with assignment numbering). The CH2′/2″ and CH5′/5″ peak positions are folded in from their normal positions around 40 and 66 ppm, respectively. Their proper chemical shift values are indicated in Table S1. CH3′ resonances were not assignable due to water suppression. Inset shows a zoom in of the aromatic assignments. Note that the two strands of the duplex are chemically equivalent and, therefore, have identical chemical shifts. (b) ^{1}H−^{1}H NOESY experiment with a mixing time of 320 ms showing the aromatic H8/H6 to ribose H1′ connectivites. The NOESY "walk" through the B-form helix is indicated with red lines, an example of which is shown on the structure of a B-form helix (PDB: 1N1K[1]) to the right.

better with the chemical shift difference between the ^{13}C, ^{1}H HSQC peaks of the d(CpG)$_3$ at 42 °C (folded) and 70 °C (unfolded, Figure 5B, R^2 = 0.99).

The 8mG4 r(CpG)$_3$ construct is also in slow exchange between the A- and Z-conformations (Figure 6A), albeit with an A-form population of 50.5 ± 5.3% (Table 4). This significant decrease in the population of Z-form compared to the 8mG4 d(CpG)$_3$ construct is likely a reflection of the differences in C2′-endo sugar pucker stability in DNA vs RNA.[62] The addition of 100 mM $NaClO_4$ stabilizes the Z-RNA state, decreasing the A-form population to 26.6 ± 4.0% (Figure 6A, Table 4). Similar to the d(CpG)$_3$ construct, the extracted excited state chemical shift differences from the Off-Resonance $R1_\rho$ experiments measured on the r(CpG)$_3$ duplex at 42 °C agree much better with a melted duplex (R^2 = 0.97) than with the stabilized Z-conformation (Figure 6B, R^2 = 0.63). They also poorly correlate with the chemical shift differences between the r(CpG)$_3$ construct in low- (25 mM NaCl, A-form) and high-salt (Z-form, 6 M $NaClO_4$), showing that this poor correlation is not due to the chemical shift deviations due to the 8-methyl guanine modification (Figure S19, R^2 = 0.87).

Overall, we conclude that the excited states observed in the off-resonance $R1_\rho$ experiments measured on the d(CpG)$_3$ and r(CpG)$_3$ duplexes at 42 °C most likely represent transiently unfolded states and not Z-form adoption. This is supported by the observation that the excited state chemical shift values for the purine C8 and pyrimidine C6 atoms of the d(CpG)$_3$, d(5mCpG)$_3$, and r(CpG)$_3$ constructs are all downfield by similar magnitudes (Table 2), which occurs for duplex melting (Figures 5A and 6A). This contrasts with the Z-conformation, where the aromatic C8 atoms of purines in the syn conformation are significantly more deshielded compared to the C6 atoms of the cytosines (Figures 5A, 6A and S14). In fact, our results are very similar to a previous study which investigated hybridization kinetics of unmodified and m^{6}A-modified duplexes by Off-Resonance $R1_\rho$.[73]

In addition, the 5-methyl cytosine modification has a well-known stabilizing effect on the temperature-dependent melting of DNA.[74−76] The excited state measured by off-resonance $R1_\rho$ for the d(5mCpG)$_3$ duplex has a population of 2% compared to the 4% observed for its nonmethylated counterpart (Table 2), again supporting that the identity of the minor state is indeed duplex melting. We also measured off-resonance $R1_\rho$ on

https://doi.org/10.1021/jacs.3c10406
J. Am. Chem. Soc. 2024, 146, 677−694

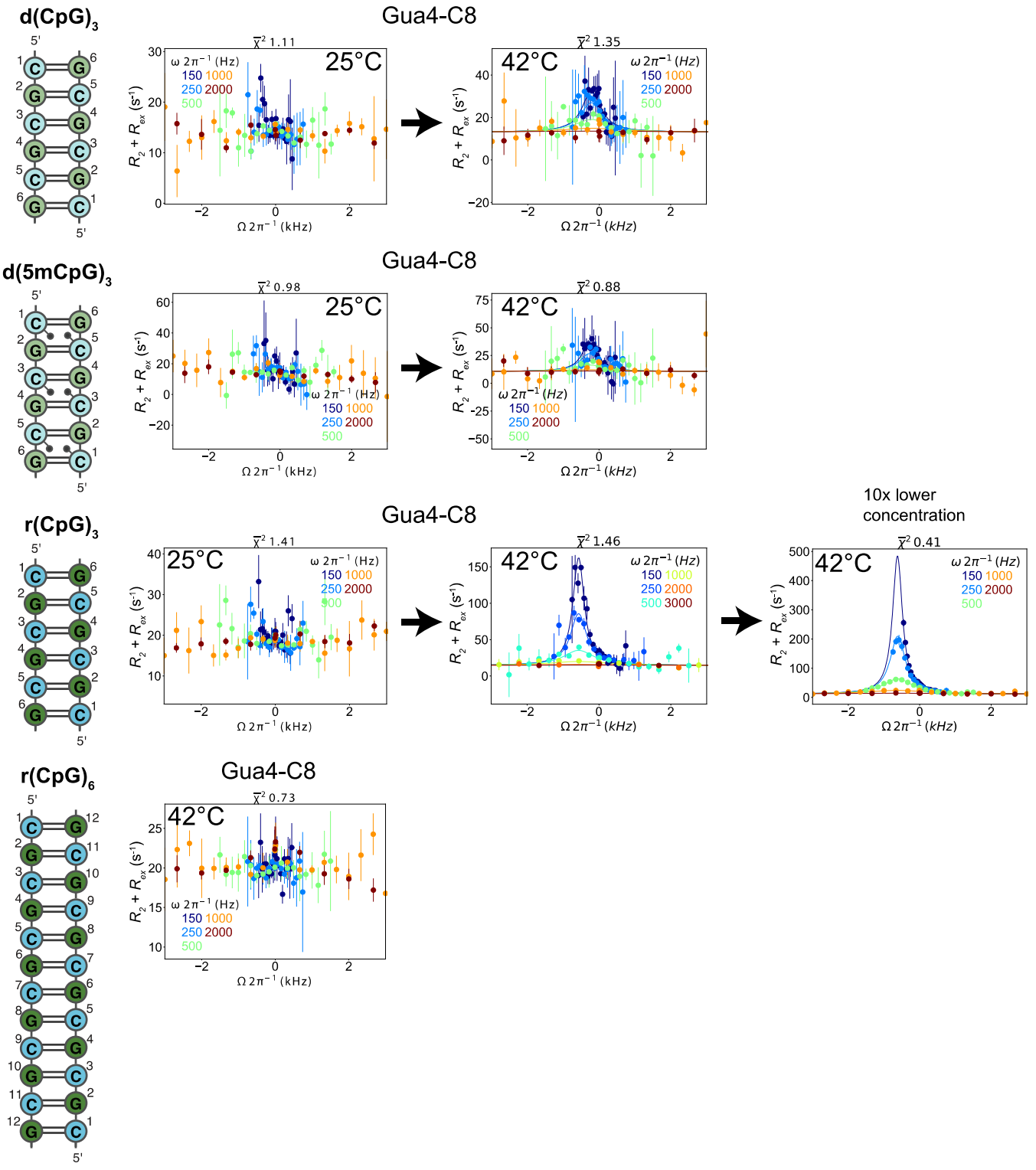

Figure 4. Off-Resonance $R1_\rho$ relaxation dispersion profiles of the different DNA and RNA constructs at 25 and 42 °C. 2D representations of the d(CpG) and r(CpG) constructs and corresponding Off-Resonance $R1_\rho$ relaxation dispersion profiles for the C8 atom of Gua4 carried out at five different spin-lock powers (150, 250, 500, 1000, and 2000 Hz, colored coded according to the legend within each plot) at 25 and 42 °C are shown to the right. The dispersion profile at 10x lower concentration of duplex for the $r(CpG)_3$ construct is also shown. $R_2 + R_{2ex}$ $(=(R1_\rho - R_1\cos^2\theta)/\sin^2\theta$, where $\theta = \tan^{-1}$ (lock power/offset)) values are given as a function of the resonance offset from the major state ($\Omega_{off}/2\pi$). Error bars represent experimental uncertainty from a bootstrapping method, as described in the Methods section. The fits (solid lines) were carried out as described in the materials and methods, and fitted parameters are found in Tables 2 and 3.

a $r(CpG)_6$ duplex at 42 °C, which is double the length of the $r(CpG)_3$ and, therefore, has a significantly higher melting temperature (Figures 4 and S18). If the excited state observed for $r(CpG)_3$ was truly a Z-conformation, it would be plausible to anticipate an excited state for the $r(CpG)_6$. This arises from the fact that the Z-form activation energy was previously

https://doi.org/10.1021/jacs.3c10406
J. Am. Chem. Soc. 2024, 146, 677−694

Table 2. Conformational Exchange Parameters from Off-Resonance $R1_\rho$ Relaxation Dispersion Experiments for Tested Constructs Using a Global Fitting Routine[a]

construct	residue/Atom identity	temperature (°C)	k_{ex} (s^{-1})	p_E (%)	Δ_ω (ppm)
$d(CpG)_3$	Gua2/C8	42	1630 ± 140	4.0 ± 0.6	1.35 ± 0.12
	Cyt3/C6	42	1630 ± 140	4.0 ± 0.6	0.87 ± 0.07
	Gua4/C8	42	1630 ± 140	4.0 ± 0.6	1.11 ± 0.09
	Cyt5/C6	42	1630 ± 140	4.0 ± 0.6	0.91 ± 0.08
$d(5mCpG)_3$	Cyt3/C6	42	1300 ± 280	2.0 ± 0.5	1.32 ± 0.25
	Gua4/C8	42	1300 ± 280	2.0 ± 0.5	1.69 ± 0.22
	Cyt5/C6	42	1300 ± 280	1.93 ± 0.06	1.18 ± 0.21
$r(CpG)_3$	Gua2/C8	42	977 ± 53	1.93 ± 0.06	2.17 ± 0.08
	Cyt3/C6	42	977 ± 53	1.93 ± 0.06	2.20 ± 0.07
	Gua4/C8	42	977 ± 53	1.93 ± 0.06	3.76 ± 0.07
	Cyt5/C6	42	977 ± 53	1.93 ± 0.06	2.45 ± 0.06
	Gua6/C8	42	977 ± 53	1.93 ± 0.06	2.47 ± 0.06

[a]Only exchange parameters for profiles that could be fit reliably are shown.

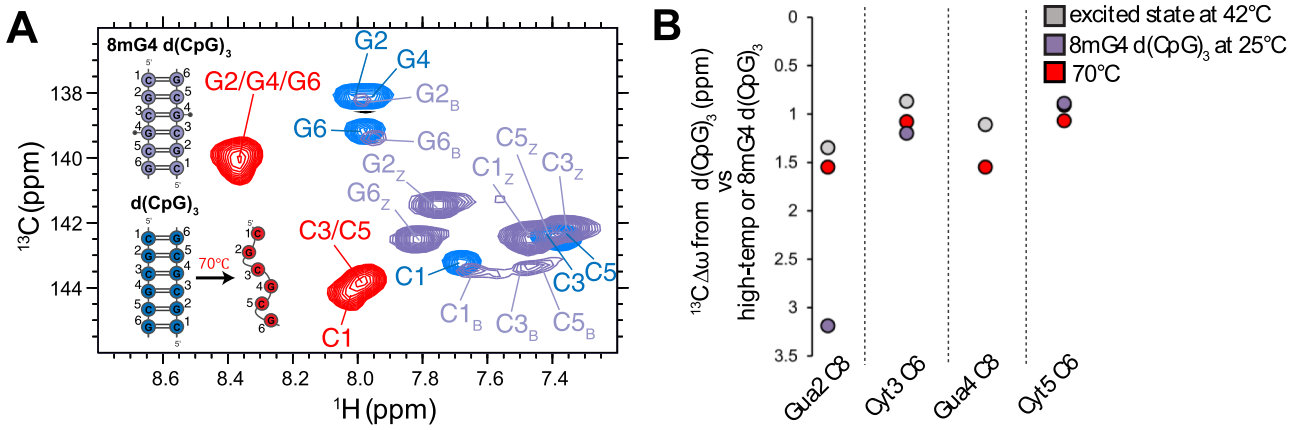

Figure 5. Identification of excited state chemical shift differences extracted from off-resonance $R1_\rho$ experiments measured on the $d(CpG)_3$. (a) Aromatic $^{13}C-^1H$ HSQC (CH8 of purines and CH6 of pyrimidines) assignments are shown for 8mG4 $d(CpG)_3$ (purple peaks, B-form and Z-form peaks are denoted by subscripts B or Z, respectively) compared to the $d(CpG)_3$ construct at 42 °C (folded, blue peaks) and 70 °C (melted, red peaks). (b) Chemical shift differences (^{13}C $\Delta\omega$) extracted from Off-Resonance $R1_\rho$ experiments measured on the $d(CpG)_3$ construct at 42 °C, the difference between the B-form and Z-form peaks in the ^{13}C, ^1H HSQC of the 8mG4 $d(CpG)_3$ construct, and the difference between the folded and melted peaks in the ^{13}C, ^1H HSQC of the $d(CpG)_3$ construct at 42 and 70 °C. The Z-form chemical shift position for Guanine 4 for the 8mG4 $d(CpG)_3$ construct could not be compared due to the methyl modification.

Table 3. B- and Z-Form Populations in the 8mG4 $d(CpG)_3$ Constructs at Different Temperatures Determined from Peak Volume Integration

residue/atom identity	B-form population (%) at 5°C	B-form population (%) at 15°C	B-form population (%) at 20°C	B-form population (%) at 25°C	B-form population (%) at 30°C	B-form population (%) at 35°C
Cyt1/C1′	12.5	14.0	13.3	9.3	3.9	2.9
Gua2/C1′	17.3	14.8	16.5	10.3	9.4	2.7
Gua2/C8	16.9	10.7	7.9	4.9	1.3	0.51
Gua6/C8	11.1	9.6	8.8	8.8	0.82	0.36
average	14.4 ± 3.1	12.3 ± 2.5	11.6 ± 4.0	8.3 ± 2.3	3.9 ± 3.9	1.6 ± 1.4

determined to be independent of chain-length,[23] whereas transient melting should no longer be observable. However, we observe no evidence of an excited state in the $r(CpG)_6$ duplex at 42 °C. Finally, the population and k_{EX} of the excited state in the $r(CpG)_3$ construct grow/decrease from 1. ± 0.1% and 977 ± 53 s^{-1} at 3.6 mM to 6.5 ± 0.6% and 513 ± 59 s^{-1} at 300 μM (Figure 4, Table 5), which is also in line with the known concentration dependence of the melting temperature in nucleic acid duplexes.[77]

Transient Melting Promotes Z-Conformation Adoption in the Presence of Zα. Most Z-conformation adoption models assume a high-energy nucleation event before helical handedness reversal and Z-form stabilization[21] (Figure 1B). In addition, we previously observed that Z-RNA adoption within the context of A-Z junctions occurred more readily when the Z-RNA stretch was flanked by internal loops or wobble base pairs.[40] Therefore, we wondered whether the transient melted state observed by NMR in the $d(CpG)_3$, $d(5mCpG)_3$, and $r(CpG)_3$ constructs could play a significant role in Z-form adoption in the presence of Zα domains. Particularly, we hypothesized that increasing the probability of transient duplex melting would promote the rate of Z-form adoption by Zα. To investigate this question, we employed circular dichroism (CD) spectroscopy, a technique which has been used

https://doi.org/10.1021/jacs.3c10406
J. Am. Chem. Soc. 2024, 146, 677−694

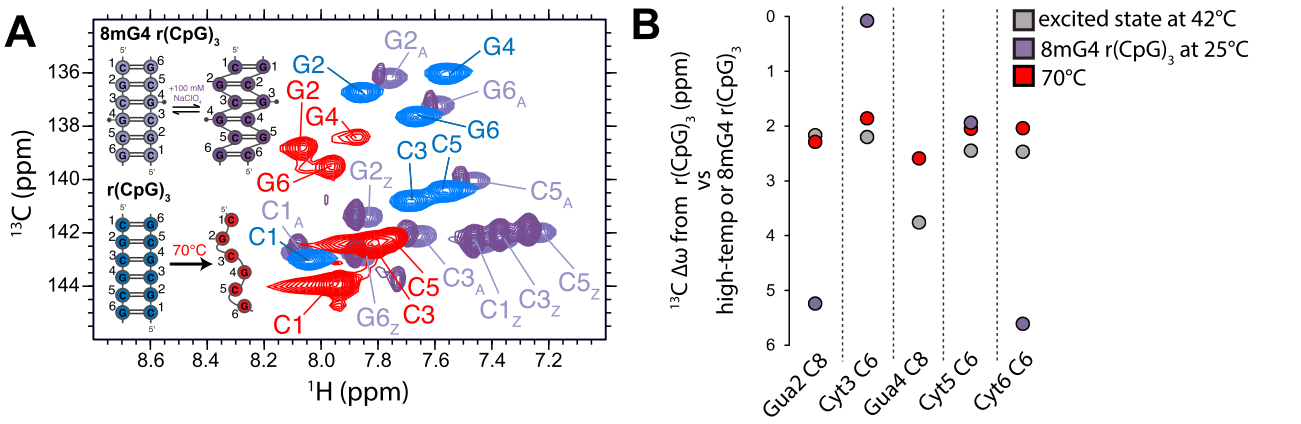

Figure 6. Identification of excited state chemical shift difference extracted from off-resonance $R1_\rho$ experiments measured on the r(CpG)$_3$ construct. (a) Aromatic ^{13}C−^{1}H HSQC (CH8 of purines and CH6 of pyrimidines) assignments are shown for 8mG4 r(CpG)$_3$ (purple peaks, A-form and Z-form peaks are denoted by subscript A and Z, respectively) compared to the r(CpG)$_3$ construct at 42 °C (folded, blue peaks) and 70 °C (melted, red peaks). For the 8mG4 r(CpG)$_3$ duplex, the addition of 100 mM $NaClO_4$ promotes the population of Z-RNA while decreasing the population of A-RNA (dark purple peaks). (b) Chemical shift differences (^{13}C $\Delta\omega$) extracted from off-resonance $R1_\rho$ experiments measured on the r(CpG)$_3$ construct at 42 °C, the difference between the A-form and Z-form peaks in the ^{13}C, ^{1}H HSQC of the 8mG4 r(CpG)$_3$ construct, and the difference between the folded and melted peaks in the ^{13}C, ^{1}H HSQC of the r(CpG)$_3$ construct at 42 and 70 °C. The Z-form chemical shift position for guanine 4 for the 8mG4 r(CpG)$_3$ construct could not be compared due to the methyl modification.

Table 4. A- and Z-Form Populations in the 8mG4 r(CpG)$_3$ Constructs at Different Temperatures Determined from Peak Volume Integration

residue/Atom identity	A-form population (%) at 5°C	A-form population (%) at 15°C	A-form population (%) at 25°C	A-form population (%) at 35°C	A-form population (%) at 45°C	A-form population (%) at 25 °C (100 mM $NaClO_4$)
Cyt1/C5	41.3	49.6	43.7	18.4	17.1	23.3
Cyt1/C6	44.1	55.8	54.9	24.5	14.9	26.4
Gua2/C8	40.6	40.3	50.8	39.0		26.3
Cyt3/C5	40.9	50.1	41.3	18.5		20.2
Cyt3/C6	48.1	55.8	47.7	42.4		28.3
Cyt5/C1′	67.7	56.72	49.7	45.9		34.2
Cyt5/C5′	48.2	51.4	50.0	15.9		27.4
Cyt5/C5″	49.2	54.2	51.2	29.7		26.4
Cyt5/C5	51.6	51.2	56.2			
Cyt5/C6	44.5	54.7	60.0	49.5		
Gua6/C8	41.0	49.5	49.7	29.5		
average	47.0 ± 7.84	51.8 ± 4.6	50.5 ± 5.3	31.3 ± 12.2	16.0 ± 1.5	26.6 ± 4.0

Table 5. Conformational Exchange Parameters From Off-Resonance $R1_\rho$ Relaxation Dispersion Experiments for the r(CpG)$_3$ Construct at 3 mM and 300 μM

construct	residue/atom identity	temperature (°C)	k_{ex} (s^{-1})	p_E (%)	Δ_ω (ppm)
3.6 mM r(CpG)$_3$	Gua4/C8	42	977 ± 53	1.9 ± 0.1	3.76 ± 0.07
300 μM ^{15}N, ^{13}C G4 r(CpG)$_3$	Gua4/C8	42	513 ± 59	6.5 ± 0.6	4.14 ± 0.07

extensively to study both Z-DNA and Z-RNA conversion.[36,40,78,79] The B-form, A-form, and Z-form of nucleic acids have unique CD absorbance patterns[80,81] in the 220−320 nm range with minimal interference from protein signal, making it ideal to track Z-form adoption in the presence of Zα (Figure S20).

We designed and tested a series of DNA and RNA duplexes that have different levels of duplex stability (depicted in Figure S21) and confirmed their ability or inability to adopt the Z-conformation in high-salt and in 1:2n (RNA:protein, where n is the number of binding sites) complex with Zα (Figure S22, salt midpoints can be found in Figure S2, Table 1). We next followed the conversion of these duplexes to the Z-form as a function of time and at different temperatures after adding saturating amounts of Zα (as depicted in Figure S20, results in Figures 7, S23 and Table 6).

Our NMR results showed that the r(CpG)$_3$ construct displayed transient duplex unfolding while the r(CpG)$_6$ construct did not. Therefore, we decided to test how duplex length (6, 12, and 24 bp CpG DNA and RNA duplexes, depicted in Figure S21) plays a role in Z-DNA and Z-RNA adoption rates in the presence of Zα. It has been previously shown that Z-form adoption is promoted as chain-length is increased in poly d(CpG)$_n$ constructs, with the rationale being that longer chains have more potential sites for high-energy nucleation events to occur thereby promoting Z-form adoption.[23] However, the duplex length was only able to be crudely estimated, and only two lengths were tested (a 24 and

https://doi.org/10.1021/jacs.3c10406
J. Am. Chem. Soc. 2024, 146, 677−694

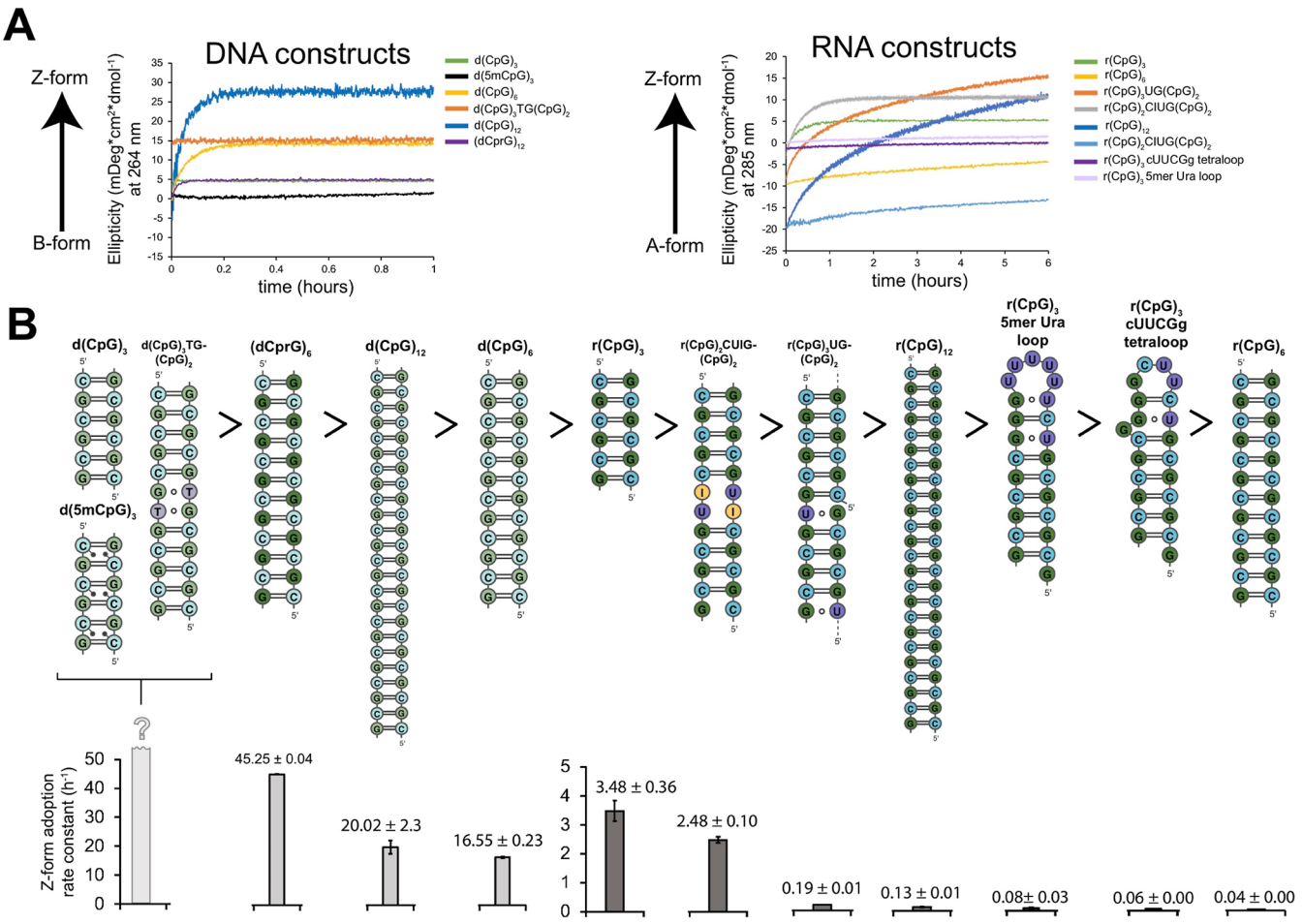

Figure 7. Z-form adoption rates in DNA and RNA constructs. (a) Circular dichroism time-course experiments showing the rate of Z-DNA (tracked at 264 nm) and Z-RNA (tracked at 285 nm) adoption after the addition of saturating concentrations of Zα at 25 °C. The different constructs are color-coded according to the legend on the right-handed side. (b) 2D depictions of DNA and RNA constructs (above) are shown in descending order according to their Z-form adoption rates at 25 °C (below), with their rate constants per hour indicated.

580 bp duplex), meaning that the potential effects of duplex melting due to temperature may have been missed.

We observe that the shorter 6 bp $d(CpG)_3$ and $r(CpG)_3$ constructs convert to the Z-form significantly faster compared to the 12 bp ones (Figure 7). The $d(CpG)_3$ construct is already completely in the Z-conformation before we could begin the CD measurement (~5 s delay before measurement), while the $d(CpG)_6$ was converted to the Z-form with an observed rate constant (k) of 16.55 ± 0.18 h^{-1} at 25 °C (Table 6). For the RNA case, a similar phenomenon was observed with the $r(CpG)_3$ flipping to the Z-conformation 100x faster compared to the $r(CpG)_6$ with rate constants of 3.480 ± 0.025 and 0.035 ± 0.000 h^{-1} at 25 °C, respectively (Table 6). The slower kinetics observed for RNA is due to the higher energy barrier for flipping the sugar pucker into the C2′-endo conformation for RNA compared to DNA.[36,62] Interestingly, doubling the number of bps again from 12 to 24 appears to have the opposite effect, although more subtle, increasing the rates from 16.55 ± 0.18 and 0.035 ± 0.000 h^{-1} to 20.02 ± 0.38 and 0.129 ± 0.000 h^{-1}, corresponding to an increase of 1.2× and 3.7× in the rate constants for DNA and RNA CpG repeats, respectively (Table 6). This increase is likely due to an increased likelihood of nucleation events occurring within the chain as it gets longer, as measured previously.[23] Indeed, using a substoichiometric concentration of Zα for the $r(CpG)_{12}$ construct (2:1 Zα:RNA where a total of 8 Zα can bind to the $r(CpG)_{12}$) results in a similar rate constant to the fully saturated experiment at 25 °C, but results in an overall lower final population of Z-form adoption, suggesting a high-level of cooperativity (Figure 7, Table 6). The difference in the increased rates between the DNA and RNA constructs may indicate that RNA becomes more cooperative than DNA with an increasing chain-length for the constructs tested in this study. This agrees with the increased hillslope observed in the $NaClO_4$ titrations between the $r(CpG)_6$ and $r(CpG)_{12}$ constructs (hillslope factor of 1.6) compared to those between the $d(CpG)_6$ and $d(CpG)_{12}$ constructs (hillslope factor of 0.9). The rate constant becomes increasingly slower (relative to the fully saturated experiment) as the temperature increases, indicating that the lower stoichiometric amount of Zα cannot fully recapitulate the rates observed in the fully saturated experiment (Table 6), indicating pseudo first-order kinetics. We also measured time-courses for the $d(5mCpG)_3$ construct, but as with the $d(CpG)_3$ duplex, it was already in the Z-conformation before measurement could begin. Therefore, Z-form adoption occurs quickly on shorter duplexes because they more easily melt compared with longer duplexes.

However, helix length is not the only factor that impacts duplex destabilization. Next, we wanted to test whether promoting base pair opening in the $d(CpG)_6$ and $r(CpG)_6$

https://doi.org/10.1021/jacs.3c10406
J. Am. Chem. Soc. 2024, 146, 677−694

Table 6. Rate Constants and Activation Energies Extracted from Circular Dichroism Time Course Experiments[a]

construct	k (h^{-1}) at 5°C	k (h^{-1}) at 15°C	k (h^{-1}) at 20°C	k (h^{-1}) at 25°C	k (h^{-1}) at 32°C	k (h^{-1}) at 42°C	k (h^{-1}) at 50°C	k (h^{-1}) at 55°C	E_A (kcal mol^{-1})
$d(CpG)_3$	*	a		a					
$d(5mCpG)_3$	a	a		a					
$d(CpG)_6$	0.655 ± 0.009	2.768 ± 0.06		16.545 ± 0.23					26.562 ± 0.003
$d(CpG)_3TG(CpG)_2$	a	a		a					
$(dCprG)_6$	0.732 ± 0.08	8.012 ± 0.11		45.27 ± 0.04					33.990 ± 0.909
$d(CpG)_{12}$	0.716 ± 0.08	2.979 ± 0.39		20.015 ± 2.30					27.387 ± 0.045
$r(CpG)_3$		0.464 ± 0.12	0.994 ± 0.002	3.480 ± 0.36	27.06 ± 0.845	150.6 ± 22.91		811.85 ± 179.96	40.584 ± 0.343
$r(CpG)_6$				0.035 ± 0.000	0.283 ± 0.002	1.814 ± 0.35	17.685 ± 2.072	25.145 ± 2.072	42.870 ± 0.719
$r(CpG)_3UG(CpG)_2$				0.191 ± 0.007		40.625 ± 1.761		167.8 ± 57.70	44.787 ± 1.838
$r(CpG)_2CIUG(CpG)_2$		0.2038 ± 0.000	0.5982 ± 0.006	2.479 ± 0.103	17.865 ± 0.375	73.065 ± 22.154			40.735 ± 1.902
$r(CpG)_{12}$				0.129 ± 0.011	0.724 ± 0.003	7.03 ± 0.017	29.3 ± 0.024	73.75 ± 8.966	41.371 ± 0.340
$r(CpG)_{12}$ (2:1 Zα:RNA)				0.117 ± 0.024	0.432 ± 0.045	3.351 ± 1.617	8.278 ± 0.002	26.465 ± 0.332	33.705 ± 1.021
$r(CpG)_3$ cUUCGg tetraloop				0.058 ± 0.004	0.664 ± 0.021	3.099 ± 0.204	18.075 ± 1.181	42.95 ± 2.234	41.153 ± 0.507
$r(CpG)_3$ 5mer Ura loop				0.077 ± 0.026	0.654 ± 0.008	2.777 ± 0.026	17.74 ± 0.453	46.72 ± 0.084	40.050 ± 0.278

[a]= construct already completely in the Z-conformation before wavelength monitoring began.

constructs, which converted to the Z-form quite slowly, might increase their Z-adoption rate in the presence of Zα. It is well-known that TG and UG wobble base pairs within the context of B- and A-form helices result in local helical distortions, which promote base pair dynamics.[82−85] Therefore, we replaced the fourth G in the $d(CpG)_6$ and $r(CpG)_6$ constructs with either a T or U nucleotide to create TG and UG wobble base pairs, which minimally perturb Z-form structure.[86] This resulted in a DNA construct with a tandem TG wobble ($d(CpG)_3TG(CpG)_2$) and an RNA one with two UG wobbles spaced apart by 4 bps ($r(CpG)_3UG(CpG)_2$) due to a register shift of the duplex (as depicted in Figure S21), as confirmed by NMR and melting temperature measurements (Figure S24, Table 1). We confirmed that Zα is still able to convert these non CpG sequences to the Z-conformation by circular dichroism (Figure S22), as anticipated from prior X-ray crystal structures of Z-DNA with non CpG sequences.[87]

The introduction of these TG and UG wobble base pairs into the $d(CpG)_6$ and $r(CpG)_6$ constructs significantly increased their rate constants (Figures 7 and S23, Table 6). The Z-adoption rate of the $d(CpG)_3TG(CpG)_2$ duplex could no longer be measured as it was already in the Z-form before measurement could begin. The $r(CpG)_3UG(CpG)_2$ construct had a rate constant of 0.191 ± 0.000 h^{-1} at 25 °C, corresponding to a 5.5x increase compared to that of the $r(CpG)_6$ construct (Table 6).

Since A-to-I editing of AU base pairs by ADAR1 is well-known to destabilize dsRNA structures,[88−90] we also tested to see if a tandem inosine-uracil base pair insertion into the $r(CpG)_6$ would also promote Z-form adoption rates by Zα. The $r(CpG)_2CUIG(CpG)_2$ construct (depicted in Figure S21) has a very low melting temperature of 38.39 °C (Figure S3, Table 1), confirming the destabilizing effect of the tandem inosine insertion. The $r(CpG)_2CUIG(CpG)_2$ construct converted to the Z-conformation with a rate constant (k) of 2.48 ± 0.10 h^{-1} at 25 °C (Figures 7, S23, Table 6), which is 71× faster than the $r(CpG)_6$ and only 0.7× slower than the $r(CpG)_3$ constructs at the same temperature.

Finally, we wanted to investigate what the effects of capping a Z-forming sequence with loops of diverse stabilities have on its Z-form adoption rate. Therefore, we capped the $r(CpG)_3$, which adopts the Z-form relatively quickly, to make two stem-loop constructs, one with a tetraloop having the cUUCGg sequence, and another with a 5mer loop containing uracils (Figure S21). Both constructs required a high concentration of salt to adopt the Z-conformation compared to the duplex constructs (adopting the Z-form around 8 M $NaClO_4$, Figure S2). Zα binding appears to promote only a partial growth in ellipticity at 285 nm, suggesting possible A-Z junction formation (Figure S22). Following the two stem-loop's partial Z-form adoption by CD time courses showed that they have rates comparable to, albeit faster than, the $r(CpG)_6$, with the 5mer uracil loop being slightly faster than the tetraloop construct (Figures 7 and S23). Therefore, capping the $r(CpG)_3$ construct is highly inhibitive of its Z-conformation adoption rate. We speculate that this is likely due to either sterically preventing reorganization of the stem into the correct Z-form geometry or by making spontaneous melting events rarer.

Overall, these results suggest that the intrinsic ability of a duplex to melt has a significant effect on its Z-DNA/Z-RNA adoption rate. This is supported by several observations. First, doubling the base pairs from 6 to 12 (which depleted the

https://doi.org/10.1021/jacs.3c10406
J. Am. Chem. Soc. 2024, 146, 677−694

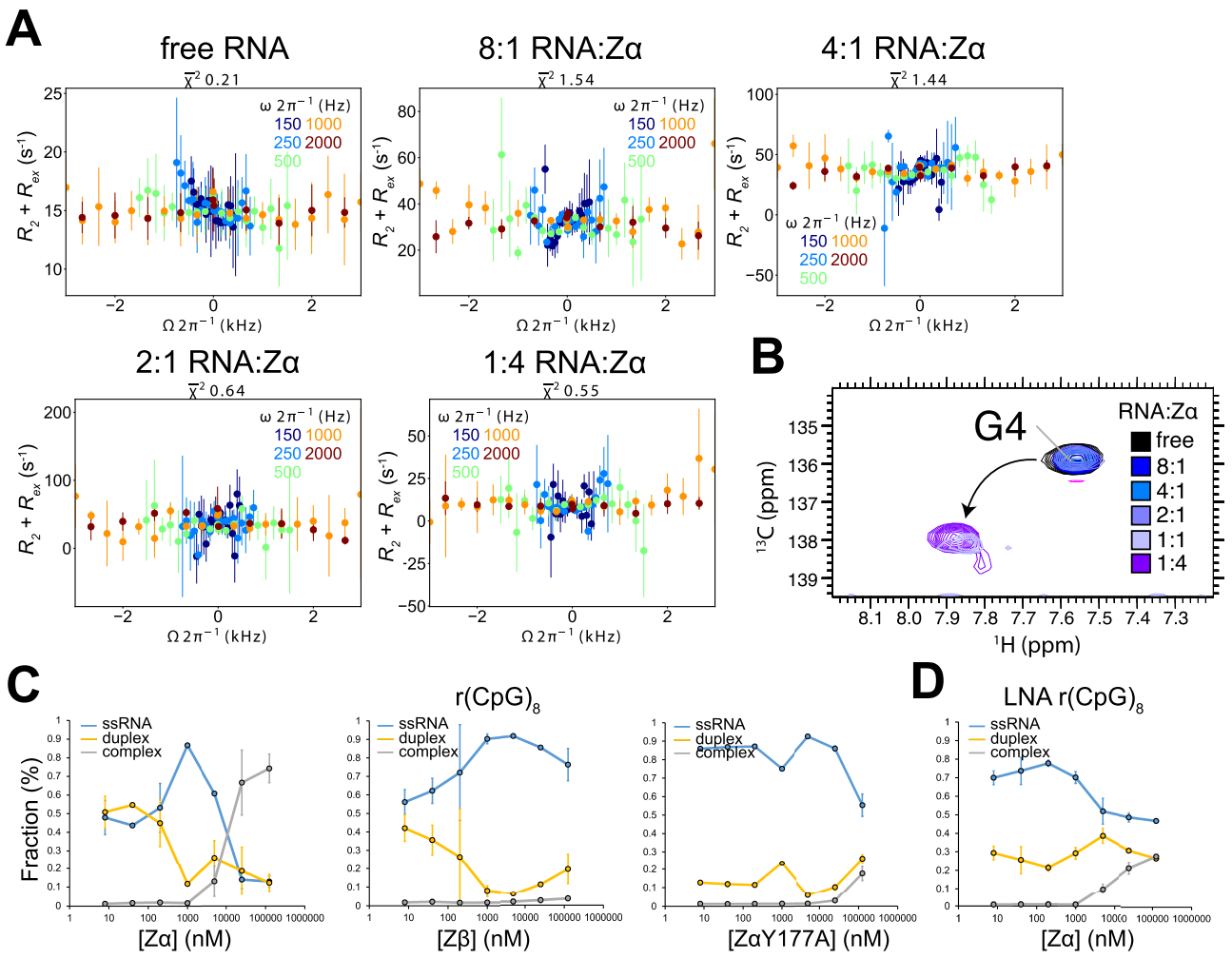

Figure 8. Characterization of exchange in the $r(CpG)_3$ construct at increasing concentrations of Zα. (a) Off-resonance $R1_\rho$ relaxation dispersion profiles for the C8 atom of isotopically labeled Gua4 in the $r(CpG)_3$ construct measured with increasing concentrations of Zα. The molar ratio of RNA/Zα can be found at the top of the graphs. Off-resonance $R1_\rho$ experiments were carried out at five different spin-lock powers (150, 250, 500, 1000, and 2000 Hz, colored coded according to the legend on the right). $R_2 + R_{ex}$ (=$R1_\rho$) values are given as a function of the resonance offset from the major state ($\Omega_{off}/2\pi$). Error bars represent experimental uncertainty. (b) ^1H,^{13}C HSQC spectra showing the C8 atom of isotopically labeled Gua4 in the $r(CpG)_3$ construct is shown at increasing concentrations of Zα, color coded according to the legend on the right. (c) The fraction of ssRNA $r(CpG)_8$, dsRNA $r(CpG)_8$, and $r(CpG)_8$ in complex with Zα, Zβ, and ZαY177A extracted from electrophoretic mobility shift assays (shown in Figure S28). The values shown are an average of two replicates plotted on a log scale. (d) Same as in (c), but with a $(CpG)_8$ LNA construct which cannot adopt the Z-conformation.

population of transient duplex melting, as seen by NMR) causes the Z-adoption rate to proceed significantly slower for both DNA and RNA. Second, converting Z-form duplexes to stem-loops has an inhibitory effect on their ability to adopt the Z-conformation. Third, promoting base pair opening dynamics by the introduction of TG, UG, and IU wobble base pairs into the B-form and A-form helices of the CpG constructs promoted an increase in the Z-form adoption rate, with the inosine insertion having a very pronounced effect. This posits the possibility that the A-to-I editing of an RNA by ADAR1 may promote Zα binding, resulting in a positive feedback loop promoting further RNA editing, which we expand on in the discussion. These results are in line with one of our previous studies, which showed that Zα preferred to bind and convert dsRNA segments flanked by internal loops and wobble base pairs.[40]

Interestingly, we also note that the 8-methyl $d(CpG)_3$ and $r(CpG)_3$ constructs, which exist in slow exchange between the B-/A- and Z-conformations, had very low melting temperatures (Table 1). While the observation is only correlational, this supports that B-/A-form helices must be destabilized for the Z-conformation to become populated.

Z-DNA and Z-RNA Formation Is a Complex Process Involving Duplex Melting and Sugar Pucker Rearrangement. Since the ease of melting an RNA or DNA duplex correlated with Z-form adoption rates in the presence of Zα, we wondered whether these constructs might have lower activation energies. The activation energy of Z-DNA and Z-RNA formation by Zα in a $d(CpG)_6$ and $r(CpG)_6$ construct was previously calculated using Arrhenius fits to be 24 and 38 kcal mol^{-1}, respectively.[36] We carried out a similar analysis for all the constructs for which we could accurately measure the Z-adoption rate at different temperatures ranging from 5 to 55 °C (Figures S23, S25 and Table 6; note that the trends observed at 25 °C still hold for the other temperatures). We measured the activation energies of $d(CpG)_6$ and $d(CpG)_{12}$ to be 26.562 ± 0.003 and 27.387 ± 0.045 kcalmol^{-1}, respectively (Table 6). For the RNA constructs, activation energies were

https://doi.org/10.1021/jacs.3c10406
J. Am. Chem. Soc. 2024, 146, 677−694

found to be 40.58 ± 0.34 ($r(CpG)_3$; in agreement with the published value[36]), 42.87 ± 0.72 ($r(CpG)_6$), 41.37 ± 0.34 ($r(CpG)_{12}$), 44.79 ± 1.84 ($r(CpG)_3UG(CpG)_2$), 40.74 ± 1.90 ($r(CpG)_2CUIG(CpG)_2$), 41.15 ± 0.51 ($r(CpG)_3$ cUUCGg tetraloop), and 40.05 ± 0.28 kcal mol^{-1} ($r(CpG)_3$ 5mer Ura loop) (Figure S25, Table 6). Therefore, despite the significant differences in the observed rate constants, the activation energies only differ significantly depending on whether the construct is DNA or RNA. These results are in agreement with an earlier study, which showed no difference in activation energy for different (CpG) chain lengths[23] and suggest that there is a higher-energy process other than duplex melting that must occur before full Z-form adoption.

We reasoned this high-energy barrier is likely the rearrangement of the sugar puckers and bases as seen in the Z-conformation, which would explain the large activation energy difference between the DNA and RNA constructs, as has been previously hypothesized.[36] If this is true, we would expect that a DNA-RNA chimera construct should have a lower activation energy barrier, with cytosines being deoxyribo (allowing them to more easily adopt the C2′-endo conformation) and guanines being ribo (which would favor the C3′-endo conformation). As predicted, we measured the activation energy of the $(dCprG)_6$ construct to be ∼10 kcal mol^{-1} lower than the $r(CpG)_6$ construct at 33.99 ± 0.91 kcal mol^{-1} (Table 6). Interestingly, the $(dCprG)_6$ construct also flips to the Z-conformation 2.7× faster than the $d(CpG)_6$ at 25 °C, which is likely due to its decreased stability as judged by its lowered T_M of 55 °C compared to the 78 °C for the $d(CpG)_6$, Table 1. In further support of the role of the sugar pucker conformation in the activation energy barrier of Z-form adoption, locking the guanosines into the C3′-endo by a methylene bridge between the 2′ oxygen and the 4′ carbon of the pentose ring (otherwise known as "locked" nucleic acid or LNA[91]) prevented the duplex $(dCpLG)_6$ (depicted in Figure S21) from flipping to the Z-form (Figures S2 and S22). This suggests that even though the guanines start and end in the C3′-endo conformation, some conformational flexibility is required during the switch from the A-to the Z-conformation or that the locked bases prevent the duplex from melting in a way that allows for a Z-like state to be adopted.

Taken together, these data show that the major energetic barrier for Z-form adoption is the conformational rearrangement of the sugar puckers and bases and is length-independent over a 24 bp span. The large differences observed for the Z-form adoption rates can be rationalized by assuming that duplex melting represents a relatively low energy barrier process that is required prior to the high-energy conformational switch.

Conversion of r(CpG) RNA to the Z-Form by Zα Occurs on a Slow Time Scale and Proceeds through a Single-Stranded Intermediate. Our data so far suggest that Z-form adoption is a multistep process involving duplex melting followed by sugar pucker rearrangement and stabilization. We wondered at what point Zα plays a role in this proposed model. Theoretically, Zα could only stabilize a Z-like state once it is adopted or it could also promote duplex melting, thereby promoting the overall Z-adoption rate. We first attempted to gain insight into this question by measuring off-resonance $R1_\rho$ experiments on the $r(CpG)_3$ where guanine 4 was isotopically labeled with ^{15}N and ^{13}C at increasing concentrations of Zα. We measured these experiments at 25 °C to avoid convolution with transient duplex melting seen at 42 °C. At all RNA/Zα tested ratios, we observed no evidence of dynamics on a μs-ms time scale (Figure 8A). Instead, Zα-dependent stabilization of Z-RNA occurs on a slow time scale, which was confirmed by the disappearance of guanine C8H8 from the A-form peak position and its reappearance at the Z-form position (without any observed chemical shift perturbations, Figure 8B). This finding is in agreement with earlier NMR titration studies which looked at the imino protons of $d(CpG)_3$ and $r(CpG)_3$ constructs upon titration of Zα, which also showed slow exchange.[46] For the 8mG4 $d(CpG)_3$ construct, which is in slow exchange between the B- and Z-conformation, we were able to measure ZZ-exchange on the C8 atoms of guanine 2 and 6 (Figure S26, Table 7). From the fits of this measurement, we extracted an exchange rate from the B- to Z-form of 24.7 ± 10.0 and 31.9 ± 11.6 s^{-1} and a backward rate (from the Z- to B-form) of 5.4 ± 1.3 and 7.8 ± 1.5 s^{-1}, for Gua2 and Gua6, respectively (Figure S26, Table 7). We carried out a similar analysis for the 8mG4 $r(CpG)_3$ construct, which revealed an exchange rate from the A-to the Z-form of 5.4 ± 1.1, 4.6 ± 0.7, and 4.8 ± 0.5 s^{-1} and a backward rate (from the Z- to the A-form) of 5.1 ± 0.7, 4.3 ± 1.0, and 5.6 ± 0.4 s^{-1} for Gua2, Cyt3, and Gua6, respectively (Figure S27, Table 8). Therefore, conversion between the B-/A-form and the Z-conformation appears to occur on a slow time scale, independently of the stabilization due to chemical modification of the duplex or Zα binding.

Table 7. Conformation Exchange Parameters for Exchange between the B- and Z-form of the 8mG4 $d(CpG)_3$ Construct Measured from ZZ-Exchange

residue	p_B (%) at 25 °C (from ratio of peak intensities)	p_B (%) at 25 °C (from ratio of k_{ex})	k_{BZ} (s^{-1}) at 25°C	k_{ZB} (s^{-1}) at 25°C
Gua2 C8	4.9	18.0 ± 11.3	24.7 ± 10.0	5.4 ± 1.3
Gua6 C8	8.8	19.6 ± 11.1	31.9 ± 11.6	7.8 ± 1.5

Table 8. Conformation Exchange Parameters for Exchange between the A- and Z-form of the 8mG4 $r(CpG)_3$ Construct Measured from ZZ-Exchange

residue	p_A (%) at 25 °C (from ratio of peak intensities)	p_A (%) at 25 °C (from ratio of K_{ex})	k_{AZ} (s^{-1}) at 25°C	k_{ZA} (s^{-1}) at 25°C
Gua2 C8	42.0	48.6	5.4 ± 1.1	5.1 ± 0.7
Cyt3 C6	40.2	48.4	4.6 ± 0.7	4.3 ± 1.0
Gua6 C8	55.1	53.7	4.8 ± 0.5	5.6 ± 0.4

Serendipitously, we discovered while carrying out electrophoretic mobility shift assays (EMSA) that the binding of Zα to an $r(CpG)_8$ construct causes the RNA to go through a single-stranded intermediate prior to Z-form adoption (Figures 8C and S28A). Under our experimental conditions, the $r(CpG)_8$ in the free form exists in equilibrium as a single-stranded and double stranded species (Figure S28A). The two bands were assigned by titrating in excess amounts of unlabeled $r(CpG)_8$, which increased the melting temperature T_M and caused the intensity of the upper band to increase (Figure S28E). In addition, running the same samples under denaturing conditions resulted in upper and lower band

https://doi.org/10.1021/jacs.3c10406
J. Am. Chem. Soc. 2024, 146, 677−694

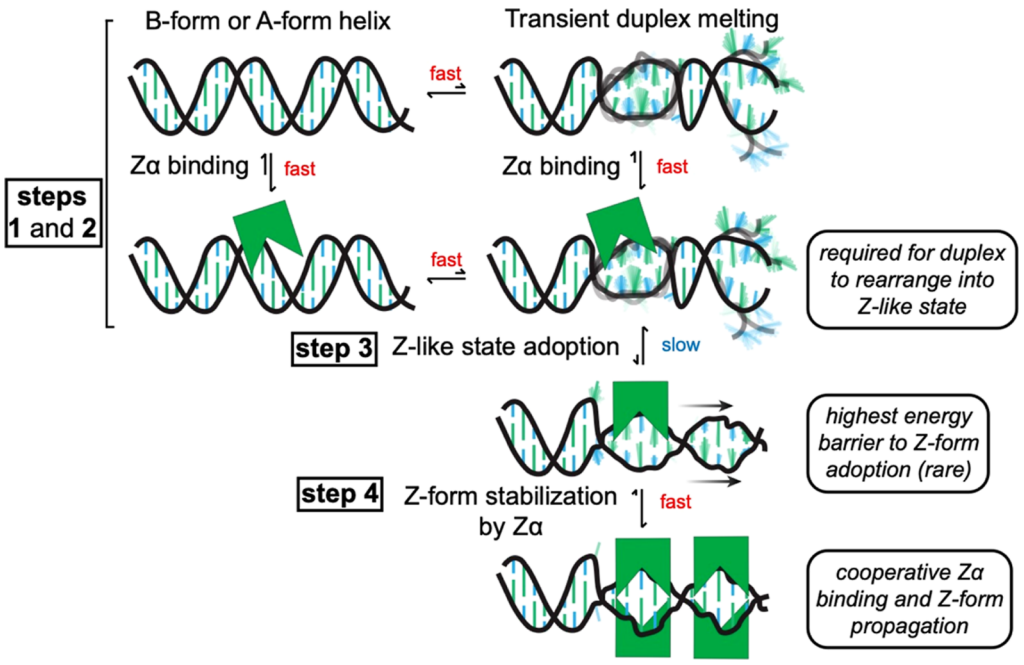

Figure 9. Model for Z-form adoption by Zα. First, Zα binds to a right-handed B- or A-form helix nonspecifically (step 1), the rates of which are dependent on the concentration of Zα domains. Next, the duplex transiently melts, which may be promoted through Zα binding (step 2). The dynamics of these steps occur on a relatively faster time scale (on the micro- to millisecond time regime). From here, the ribose sugar pucker and nucleosides have to rearrange into a high-energy, Z-like state (which occurs slowly taking seconds to hours, step 3). Then, Zα cooperatively binds to and stabilizes the Z-conformation (which occurs fast once a Z-like state is adopted, step 4).

merging, showing that they are not products of degradation (Figure S28F). This suggests that at the RNA concentration used for the EMSA (~24 pM), r$(CpG)_8$ is below the K_D needed to form stable duplexes. As the concentration of Zα is increased up to 1 μM, the dsRNA species becomes further depopulated while the ssRNA species increases, without any measurable complex formation. After 1 μM, the ssRNA species disappears, and a much higher molecular weight band appears, indicating complex formation (Figures 8C and S28A). We do not observe this phenomenon with an LNA version of $(CpG)_8$ (which cannot adopt the Z-form as showed earlier, Figure S22), with little change in the relative populations of single- and double-stranded species (Figures 8D and S28D). These results further support not only that the DNA and RNA must go through an unfolded intermediate prior to Z-form adoption but also that Zα is able to help promote this melting event at low concentrations. It is possible that we observed this activity of Zα only because the instability of the duplex species meant that melted duplexes could not immediately reform, allowing us to capture it on a gel.

Interestingly, duplex melting by the addition of Zα occurs relatively quickly as judged by an EMSA time-course, which showed no difference in the relative populations of dsRNA and ssRNA for the r$(CpG)_8$ after the addition of 1 μM Zα from 5 to 35 min (Figure S28G). Quickly spiking in 5 and 25 μM Zα after the 30 min mark does not lead to the productive formation of complex, as we observed for the full 30 min incubation with Zα (compare Figure S28G–A). This supports our circular dichroism time-course results which suggested that a second, high-energy Z-like state must be adopted after duplex melting before productive Z-form adoption can occur.

Unexpectedly, we observe a similar behavior for Zβ (structurally conserved with Zα, isoelectric point is 8.1 compared to 9.8 - and incapable of promoting Z-form) and a Zα mutant (ZαY177A, which cannot stabilize Z-DNA/Z-RNA) but without noticeable complex formation at higher protein concentrations (Figures 8C and S28B). ZαY177A shows melting activity, but it is not observable until about 5 μM protein (Figures 8C and S28C). Therefore, this suggests that the observed melting activity of Zα is not specific to its Z-form adoption activity, as it could be a general feature of positively charged helix-turn-helix domains.

Proposed Model for Z-Form Adoption by Zα. Synthesizing all the results from this study, we have constructed a model for Z-DNA and Z-RNA adoption in the presence of Zα (Figure 9). First, Zα binds nonspecifically to a B-form or A-form helix using a similar binding interface used for Z-form stabilization (Figure 9, step 1). From here, the B-/A-form helix must experience a transient duplex melting event, which is more likely to occur in the proximity of helix ends and internal loops and which Zα binding may help to promote (Figure 9, step 2). Both of these steps occur on a relatively fast time scale, with duplex melting being in the intermediate time regime (as measured by Off-resonance $R1_\rho$). After this, the strands must rearrange into a Z-like state with alternating sugar pucker and nucleobase conformations, which occurs slowly and is rate-limiting (Figure 9, step 3). This state is high-energy and is thus a rare state which is easier to adopt in DNA compared to RNA due to the difficulty in adopting the C2′-endo conformation in RNA. At this point, Zα will bind to the Z-like state with an order of magnitude higher affinity, stabilizing it into the Z-conformation and promoting the binding of additional Zα domains in a cooperative manner (Figure 9, step 4). This model has implications for the role of Zα domains in biology, which we discuss below.

https://doi.org/10.1021/jacs.3c10406
J. Am. Chem. Soc. 2024, 146, 677−694

DISCUSSION AND CONCLUSIONS

The conversion of right-handed helices to the left-handed Z-conformation is a thermodynamically challenging process[20] involving complete helical reversal and alternation of the nucleobases and (deoxy)riboses between the syn/anti and C2′/C3′-endo conformations.[4,8−11] Zα domains, found within a variety of innate immune response proteins,[35] are able to promote this conversion in double-stranded DNA and RNA simply through binding to and stabilizing the unique Z-form geometry.[6,36] This process is known to involve intermediate steps,[42−47] but the identity of these steps has remained poorly characterized.

Our off-resonance $R1_\rho$ experiments, which probe low population dynamic states,[51−53,55] showed no evidence of transiently sampled Z-conformations but did reveal that short d/r$(CpG)_3$ duplexes sampled a transiently unfolded state at 42 °C whereas a r$(CpG)_6$ construct did not (Figures 4−6). The transient melting observed in the shorter duplexes correlated with significantly faster Z-form adoption rates in the presence of Zα as measured by circular dichroism studies (Figure 7). We further investigated this phenomenon and showed that duplex stability generally played a major role in Z-form adoption rates, as was supported by our EMSA experiments (Figure 8). This was illustrated by the significantly faster Z-form adoption rates in the longer d/r$(CpG)_6$ constructs with inserted noncanonical base pairs and inosine nucleobases (Figure 7).

Interestingly, despite the different nucleic acid constructs having significantly different rate constants, the only differences in measured activation energies were between DNA and RNA, with RNA having a significantly higher energy barrier (Figure S25). This suggests that there is another, rate-limiting, step after duplex melting that likely involves adopting the proper Z-form geometry (which requires more energy for RNA due to the difficulty in adopting the C2′-endo conformation[36]).

Experimentally Validated Model for the Conversion of A/B to the Z-Conformation. From these results, we propose a model whereby Zα binds to an A-/B-form helix nonspecifically (the rate of which would depend upon Zα concentration), the helix transiently melts and adopts a Z-like state, which is then followed by stabilization of the Z-form structure in a Zα-dependent manner (Figure 9). This model is very similar to the previously proposed zipper model[31] but also takes into account the role of Zα domains and provides experimental evidence that the high-energy nucleation event described in the zipper model is likely duplex unfolding. We believe that this makes sense from a biochemical and structural perspective, as the intuitively most straightforward path to convert from a right-handed to a left-handed helix would be to locally dissociate the two right-handed and base-paired strands from each other and reanneal them together in the left-handed conformation. This would also explain why B−Z junction adoption was previously shown to occur much more quickly than Z-DNA by itself,[92] as the favorable entropic energy gain from the creation of the junctions between B-DNA/A-RNA and Z-form sequences likely allows for the strands to dissociate and reform into the Z-conformation more easily.

Does Zα Stabilize Z-Conformations via an Active or Passive Mechanism? One open question in the field is determining whether Zα domains play an "active" or "passive" role in Z-form adoption. That is, whether Zα domains recognize presampled Z-conformations and subsequently stabilize them (the passive mechanism[49]) or whether binding of Zα to DNA/RNA pushes the helix into the Z-form (the active mechanism[42−44,46]). There is evidence for both models of Z-DNA/RNA adoption.[42−48,50] Our data suggest that two of the intermediate states in the pathway to Z-form adoption are duplex melting and conformational rearrangement into a Z-like state (Figure 9). In addition, we showed that Zα likely stabilizes a Z-like state which is adopted prior to full Z-conformation stabilization, which occurs on a slow time scale. Our data do not allow us to conclude definitively whether this state is adopted independently or if Zα is required to push the nucleic acid into this state once the duplex is melted. Through our off resonance $R1_\rho$ data, we detected only the presence of transient melting of our duplex constructs in the absence of Zα. This suggests that a possible transient Z-like state is either outside of the time scale measurable by off resonance $R1_\rho$, or that the state is exceedingly rare and Zα is required for its adoption. However, by comparing the A-form peak intensities of the isotopically labeled r$(CpG)_3$ construct to the noise level where the Z-form peak would be expected to be (under the slow exchange limit) at 25 °C, the Z-conformation population cannot be more than 0.08%. If transient Z-form adoption occurs on a slow time scale, this would mean that it is a rare state under low salt conditions and without divalent metal ions. One possible interpretation of the lack of an intermediate state being populated with the addition of Zα is that it simply stabilizes this rare state and therefore plays a passive role in Z-form adoption.

Because transient Z-form adoption is rare under the conditions we tested, we do not expect the Z-conformation to be populated at a significant level in the cell in the absence of Zα or other stabilizing factors such as chemical modifications, buffer conditions, torsional/mechanical stress,[93,94] or other potential unknown conditions. A Z-conformation may not be adopted to an appreciable degree without the binding of Zα. Therefore, Z-conformation adoption due to the presence of Zα can also be thought of as an active mechanism, especially considering that Zα binds to A-form helices prior to Z-form adoption (as evidenced by the binding of Zα to the $(CpG)_8$ LNA, Figure S28D). Therefore, Z-form adoption may have aspects of both an active and a passive mechanism, with the protein being bound to the nucleic acid prior to the flip, but still requiring a transient Z-like state to be adopted before full stabilization. However, that is not to say that Zα-dependent stabilization of Z-conformations always proceeds by a combined active/passive mechanism. For prestabilized Z-form duplexes, Zα would likely immediately recognize and bind to the Z-form state, invoking a purely passive binding mechanism.

Does A-to-I Editing by ADAR1 Induce Z-RNA? Adenosine deaminase acting on RNA 1 (ADAR1) is an A-to-I editase which regulates the innate immune response by preventing activation of dsRNA sensors.[35,56] The longer isoform of ADAR1 contains an N-terminal Zα domain, which has been shown to play an important role in ADAR1's function.[39,95,96] Our finding that inosylation of the r$(CpG)_6$ construct increased its Z-form adoption rate to a comparable level as that of the r$(CpG)_3$ was striking. Based on this result, we speculate that the A-to-I editing activity of ADAR1 could promote Z-RNA adoption in ADAR1's substrates which could in turn facilitate Zα binding and further A-to-I editing, helping to alleviate the loss of A-to-I editing activity observed on

https://doi.org/10.1021/jacs.3c10406
J. Am. Chem. Soc. 2024, 146, 677−694

shorter dsRNA segments.[97] This model could partially explain ADAR1p150s higher overall A-to-I editing activity[98−100] and its significantly enhanced editing of substrates containing (CpG) repeat sequences.[101]

Another mechanism which would lead to the same result is that the increased Z-RNA adoption due to A-to-I editing activity does not promote further editing, but instead helps further shield the RNA from dsRNA sensors[102] by converting potential substrates into a conformation that is not readily recognizable by their typical A-form binding domains. Since the Zα domain would act in cis with the deaminase domain within ADAR1, it would likely also be able to outcompete ZBP1[103−105] for binding to the Z-form targets it helps to create.

Under What Cellular Contexts Would Z-Conformations be Predicted to Form? Extrapolating from our findings, we predict that Z-conformations would be more likely to form in dsRNAs containing many noncanonical base pairs, internal loops, or editing events that help to partially destabilize the double-stranded character of the RNA segment. This would allow for the Z-conformation to be adopted more easily and thus promote Zα binding. These sequence elements are quite common in long dsRNA formed from repetitive elements,[104−106] such as Alu elements in humans and viral RNAs.[107−109] However, too many destabilizing base pairs would eventually cause the adopted Z-conformation to also become destabilized.[9] This would also be impacted by the number of pyrimidine-purine repeats, which determine the final stability of the adopted Z-conformation.[9] Therefore, there is likely a balance between the ease of helix melting and the stability of the adopted Z-conformation, which determines the adoption rate and overall longevity of Z-conformations in the cell. In addition to the RNA sequence itself, many potential trans-acting factors would also be predicted to promote Z-form adoption, including helicase activity[110] and torsional/mechanical stress,[93] which would facilitate duplex melting and, therefore, promote Z-form adoption as previously hypothesized.[94]

Our results add further data to previous findings that a wide range of sequence contexts can adopt the Z-conformation[40,41] and that the process is highly cooperative. Based on these findings, we wonder whether the identity of the RNA targets is not as important as the result of converting those targets to the Z-conformation. Alu elements could be targeted because they represent one of the largest sources of dsRNA in the human transcriptome and not because they possess better Z-form adopting sequences. One potential way to investigate this question would be to determine if Alu elements are targeted for editing overproportionally compared to their relative abundance. The existence of evolutionarily conserved domains that facilitate Z-DNA and Z-RNA adoption suggests that there is a major advantage in converting double-stranded nucleic acids to the Z-conformation. For example, forcing long dsRNAs into the Z-form may be a potent mechanism to avoid triggering certain dsRNA sensors, which would have otherwise recognized the long tracts of the A-form helices. Alternatively, perhaps converting dsRNA into the Z-form could act as a mechanism to evict A-form binding proteins, thereby promoting even further Zα binding and amplifying the signal of whichever Zα-containing protein is coating a particular RNA.

■ ASSOCIATED CONTENT

Supporting Information

The Supporting Information is available free of charge at https://pubs.acs.org/doi/10.1021/jacs.3c10406.

Details of sample preparation, CD, EMSA, and NMR experiments, chemical shift assignments, $R1_\rho$ RD setup details, and profiles (PDF)

■ AUTHOR INFORMATION

Corresponding Authors

Quentin Vicens − *Department of Biochemistry and Molecular Genetics, University of Colorado Denver School of Medicine, Aurora, Colorado 80045, United States; RNA Bioscience Initiative, University of Colorado Denver School of Medicine, Aurora, Colorado 80045, United States;* Present Address: Department of Biology and Biochemistry, Center for Nuclear Receptors and Cell Signaling, University of Houston, Houston, Texas 77204, USA; orcid.org/0000-0003-3751-530X; Phone: +1 (713) 743-2696; Email: qvicens@uh.edu

Beat Vögeli − *Department of Biochemistry and Molecular Genetics, University of Colorado Denver School of Medicine, Aurora, Colorado 80045, United States;* orcid.org/0000-0003-1176-3137; Phone: +1 (303) 724-16270; Email: beat.vogeli@cuanschutz.edu

Authors

Parker J. Nichols − *Department of Biochemistry and Molecular Genetics, University of Colorado Denver School of Medicine, Aurora, Colorado 80045, United States*

Jeffrey B. Krall − *Department of Biochemistry and Molecular Genetics, University of Colorado Denver School of Medicine, Aurora, Colorado 80045, United States*

Morkos A. Henen − *Department of Biochemistry and Molecular Genetics, University of Colorado Denver School of Medicine, Aurora, Colorado 80045, United States; Faculty of Pharmacy, Mansoura University, Mansoura 35516, Egypt;* orcid.org/0000-0003-4835-5583

Robb Welty − *Department of Biochemistry and Molecular Genetics, University of Colorado Denver School of Medicine, Aurora, Colorado 80045, United States*

Andrea Macfadden − *Department of Biochemistry and Molecular Genetics, University of Colorado Denver School of Medicine, Aurora, Colorado 80045, United States*

Complete contact information is available at: https://pubs.acs.org/10.1021/jacs.3c10406

Funding

We gratefully acknowledge for support Jeffrey Kieft (to P.N. and Q.V.), the National Science Foundation (Award #2153787 to Q.V. and B.V.), and the National Institutes of Health (Award #1F31AI167396 to P.N.).

Notes

The authors declare no competing financial interest.

■ ACKNOWLEDGMENTS

We would like to thank Atul Rangadurai for help implementing and analyzing the off-resonance $R1_\rho$ relaxation dispersion experiments, along with the NMR facility manager David Jones.

REFERENCES

(1) Wolfram, S. Principles of Nucleic Acid Structure, 1st ed.; Springer New York: New York, 1984.
(2) Stefl, R.; Skrisovska, L.; Allain, F. H. RNA sequence- and shape-dependent recognition by proteins in the ribonucleoprotein particle. *EMBO Rep.* **2005**, *6* (1), 33−38.
(3) Battistini, F.; Hospital, A.; Buitrago, D.; Gallego, D.; Dans, P. D.; Gelpí, J. L.; Orozco, M. How B-DNA Dynamics Decipher Sequence-Selective Protein Recognition. *J. Mol. Biol.* **2019**, *431* (19), 3845−3859.
(4) Hall, K.; Cruz, P.; Tinoco, I., Jr; Jovin, T. M.; van de Sande, J. H. 'Z-RNA'−a left-handed RNA double helix. *Nature* **1984**, *311* (5986), 584−586.
(5) Schwartz, T.; Rould, M. A.; Lowenhaupt, K.; Herbert, A.; Rich, A. Crystal Structure of the Zα Domain of the Human Editing Enzyme ADAR1 Bound to Left-Handed Z-DNA. *Science* **1999**, *284* (5421), 1841−1845.
(6) Placido, D.; Brown, B. A.; Lowenhaupt, K.; Rich, A.; Athanasiadis, A. A left-handed RNA double helix bound by the Z alpha domain of the RNA-editing enzyme ADAR1. *Structure* **2007**, *15* (4), 395−404.
(7) Popenda, M.; Milecki, J.; Adamiak, R. W. High salt solution structure of a left-handed RNA double helix. *Nucleic Acids Res.* **2004**, *32* (13), 4044.
(8) Wang, A. H.; Quigley, G. J.; Kolpak, F. J.; Crawford, J. L.; van Boom, J. H.; van der Marel, G.; Rich, A. Molecular structure of a left-handed double helical DNA fragment at atomic resolution. *Nature* **1979**, *282* (5740), 680−686.
(9) Krall, J. B.; Nichols, P. J.; Henen, M. A.; Vicens, Q.; Vögeli, B. Structure and Formation of Z-DNA and Z-RNA. *Molecules* **2023**, *28* (2), 843.
(10) Ho, P. S.; Mooers, B. H. Z-DNA crystallography. *Biopolymers* **1997**, *44* (1), 65−90.
(11) Wang, A. H. J.; Quigley, G. J.; Kolpak, F. J.; van der Marel, G.; van Boom, J. H.; Rich, A. Left-handed double helical DNA: variations in the backbone conformation. *Science* **1981**, *211* (4478), 171.
(12) Zirbel, C. L.; Auffinger, P. Lone Pair...π Contacts and Structure Signatures of r(UNCG) Tetraloops, Z-Turns, and Z-Steps: A WebFR3D Survey. *Molecules* **2022**, *27* (14), 4365.
(13) Kruse, H.; Mrazikova, K.; D'Ascenzo, L.; Sponer, J.; Auffinger, P. Short but Weak: The Z-DNA Lone-Pair···π Conundrum Challenges Standard Carbon Van der Waals Radii. *Angew. Chem., Int. Ed. Engl.* **2020**, *59* (38), 16553−16560.
(14) Sponer, J.; Gabb, H. A.; Leszczynski, J.; Hobza, P. Base-base and deoxyribose-base stacking interactions in B-DNA and Z-DNA: a quantum-chemical study. *Biophys. J.* **1997**, *73* (1), 76−87.
(15) Kollman, P. A.; Weiner, P. K.; Dearing, A. Theoretical studies of the structure and energies of base-paired nucleotides and the dissociation kinetics of a proflavine-dinucleotide complex. *Ann. N.Y. Acad. Sci.* **1981**, *367*, 250−268.
(16) Guéron, M.; Demaret, J. P. A simple explanation of the electrostatics of the B-to-Z transition of DNA. *Proc. Natl. Acad. Sci. U.S.A.* **1992**, *89* (13), 5740.
(17) Misra, V. K.; Honig, B. The electrostatic contribution to the B to Z transition of DNA. *Biochemistry* **1996**, *35* (4), 1115−1124.
(18) Guéron, M.; Demaret, J.; Filoche, M. A unified theory of the B-Z transition of DNA in high and low concentrations of multivalent ions. *Biophys. J.* **2000**, *78* (2), 1070−1083.
(19) Harvey, S. C. DNA structural dynamics: longitudinal breathing as a possible mechanism for the B ⇄ Z transition. *Nucleic Acids Res.* **1983**, *11* (14), 4867−4878.
(20) Jovin, T.; Soumpasis, D. M.; McIntosh, L. P. The Transition Between B-DNA And Z-DNA. *Annu. Rev. Phys. Chem.* **1987**, *38*, 521−558.
(21) Fuertes, M. A.; Cepeda, V.; Alonso, C.; Pérez, J. M. Molecular Mechanisms for the B−Z Transition in the Example of Poly[d(G−C)·d(G−C)] Polymers. A Critical Review. *Crit. Rev. Anal. Chem.* **2006**, *106* (6), 2045−2064.
(22) Ha, S. C.; Lowenhaupt, K.; Rich, A.; Kim, Y. G.; Kim, K. K. Crystal structure of a junction between B-DNA and Z-DNA reveals two extruded bases. *Nature* **2005**, *437* (7062), 1183−1186.
(23) Pohl, F. M.; Jovin, T. M. Salt-induced co-operative conformational change of a synthetic DNA: equilibrium and kinetic studies with poly (dG-dC). *J. Mol. Biol.* **1972**, *67* (3), 375−396.
(24) Pohl, F. M. Salt-induced transition between two double-helical forms of oligo (dC-dG). *Cold Spring Harbor Symp. Quant. Biol.* **1983**, *47*, 113−117.
(25) Goto, S. Characterization of intermediate conformational states in the B↔Z transitions of poly(dG-dC) · poly(dG-dC). *Biopolymers* **1984**, *23* (11), 2211−2222.
(26) Manzini, G.; Xodo, L. E.; Quadrifoglio, F.; van Boom, J. H.; van der Marel, G. A. dC-dG alternating oligonucleotides: thermodynamic and kinetic aspects of the B-Z transformation. *J. Biomol. Struct. Dyn.* **1987**, *4* (4), 651−662.
(27) Sundaralingam, M.; Westhof, E. Structural Motifs of the Nucleotidyl Unit and the Handedness of Polynucleotide Helices. *Int. J. Quantum Chem.* **1981**, *20*, 287−306.
(28) Chaires, J. B.; Sturtevant, J. M. Thermodynamics of the B to Z transition in poly(dGdC). *Biopolymers* **1988**, *27* (9), 1375−1387.
(29) Saenger, W.; Heinemann, U. Raison d'être and structural model for the B-Z transition of poly d(G-C).poly d(G-C). *FEBS Lett.* **1989**, *257* (2), 223−227.
(30) Ivanov, V.; Grzeskowiak, K.; Zocchi, G. Evidence for an Intermediate State in the B-to-Z Transition of DNA. *J. Phys. Chem. B* **2003**, *107* (46), 12847−12850.
(31) Ho, P. S. The non-B-DNA structure of d(CA/TG)n does not differ from that of Z-DNA. *Proc. Natl. Acad. Sci. U.S.A.* **1994**, *91* (20), 9549−9553.
(32) Lim, W.; Feng, Y. P. The stretched intermediate model of B-Z DNA transition. *Biophys. J.* **2005**, *88* (3), 1593−1607.
(33) Czarny, R. S.; Ho, P. S. Thermogenomic Analysis of Left-Handed Z-DNA Propensities in Genomes. *Methods Mol. Biol.* **2023**, *2651*, 195−215.
(34) Kastenholz, M. A.; Schwartz, T. U.; Hünenberger, P. H. The transition between the B and Z conformations of DNA investigated by targeted molecular dynamics simulations with explicit solvation. *Biophys. J.* **2006**, *91* (8), 2976−2990.
(35) Nichols, P. J.; Krall, J. B.; Henen, M. A.; Vögeli, B.; Vicens, Q. Z-RNA biology: a central role in the innate immune response? *RNA* **2023**, *29* (3), 273−281.
(36) Brown, B. A., 2nd; Lowenhaupt, K.; Wilbert, C. M.; Hanlon, E. B.; Rich, A. The Zα domain of the editing enzyme dsRNA adenosine deaminase binds left-handed Z-RNA as well as Z-DNA. *Proc. Natl. Acad. Sci. U.S.A.* **2000**, *97* (25), 13532−13536.
(37) Langeberg, C. J.; Nichols, P. J.; Henen, M. A.; Vicens, Q.; Vögeli, B. Differential Structural Features of Two Mutant ADAR1p150 Zα Domains Associated with Aicardi-Goutières Syndrome. *J. Mol. Biol.* **2023**, *435* (8), 168040.
(38) Schade, M.; Turner, C. J.; Lowenhaupt, K.; Rich, A.; Herbert, A. Structure-function analysis of the Z-DNA-binding domain Zalpha of dsRNA adenosine deaminase type I reveals similarity to the (alpha +beta) family of helix-turn-helix proteins. *EMBO J.* **1999**, *18* (2), 470.
(39) Nakahama, T.; Kato, Y.; Shibuya, T.; Inoue, M.; Kim, J. I.; Vongpipatana, T.; Todo, H.; Xing, Y.; Kawahara, Y. Mutations in the adenosine deaminase ADAR1 that prevent endogenous Z-RNA binding induce Aicardi-Goutières-syndrome-like encephalopathy. *Immunity* **2021**, *54* (9), 1976−1988.e7.
(40) Nichols, P. J.; Bevers, S.; Henen, M.; Kieft, J. S.; Vicens, Q.; Vögeli, B. Recognition of non-CpG repeats in Alu and ribosomal RNAs by the Z-RNA binding domain of ADAR1 induces A-Z junctions. *Nat. Commun.* **2021**, *12* (1), 793.
(41) Feng, S.; Li, H.; Zhao, J.; Pervushin, K.; Lowenhaupt, K.; Schwartz, T. U.; Dröge, P. Alternate rRNA secondary structures as regulators of translation. *Nat. Struct. Mol. Biol.* **2011**, *18* (2), 169−176.
(42) Kang, Y. M.; Bang, J.; Lee, E. H.; Ahn, H. C.; Seo, Y. J.; Kim, K. K.; Kim, Y. G.; Choi, B. S.; Lee, J. H. NMR spectroscopic elucidation

https://doi.org/10.1021/jacs.3c10406
J. Am. Chem. Soc. 2024, 146, 677−694

of the B-Z transition of a DNA double helix induced by the Z alpha domain of human ADAR1. *J. Am. Chem. Soc.* **2009**, *131* (32), 11485−11491.
(43) Lee, A. R.; Park, C. J.; Cheong, H. K.; Ryu, K. S.; Park, J. W.; Kwon, M. Y.; Lee, J.; Kim, K. K.; Choi, B. S.; Lee, J. H. Solution structure of the Z-DNA binding domain of PKR-like protein kinase from Carassius auratus and quantitative analyses of the intermediate complex during B-Z transition. *Nucleic Acids Res.* **2016**, *44* (6), 2936−2948.
(44) Lee, E. H.; Seo, Y. J.; Kim, H. E.; Lee, Y. M.; Kim, C. M.; Lee, J. H. Population Analysis of the Intermediate Complex States During B-Z Transition of Non-CG-Repeat DNA Duplexes Induced by the Z Alpha Domain of Human ADAR1. *Bull. Korean Chem. Soc.* **2011**, *32* (2), 719−721.
(45) Kim, S. H.; Lim, S. H.; Lee, A. R.; Kwon, D. H.; Song, H. K.; Lee, J. H.; Cho, M.; Johner, A.; Lee, N. K.; Hong, S. C. Unveiling the pathway to Z-DNA in the protein-induced B-Z transition. *Nucleic Acids Res.* **2018**, *46* (8), 4129−4137.
(46) Lee, A. R.; Hwang, J.; Hur, J. H.; Ryu, K. S.; Kim, K. K.; Choi, B. S.; Kim, N. K.; Lee, J. H. NMR Dynamics Study Reveals the Zα Domain of Human ADAR1 Associates with and Dissociates from Z-RNA More Slowly than Z-DNA. *ACS Chem. Biol.* **2019**, *14* (2), 245−255.
(47) Park, C.; Zheng, X.; Park, C. Y.; Kim, J.; Lee, S. K.; Won, H.; Choi, J.; Kim, Y. G.; Choi, H. J. Dual conformational recognition by Z-DNA binding protein is important for the B-Z transition process. *Nucleic Acids Res.* **2020**, *48* (22), 12957−12971.
(48) Behe, M.; Zimmerman, S.; Felsenfeld, G. Changes in the helical repeat of poly(dG-m5dC). poly(dG-m5dC) and poly(dG-dC). poly(dG-dC) associated with the B-Z transition. *Nature* **1981**, *293* (5829), 233−235.
(49) Bae, S.; Kim, D.; Kim, K. K.; Kim, Y. G.; Hohng, S. Intrinsic Z-DNA is stabilized by the conformational selection mechanism of Z-DNA-binding proteins. *J. Am. Chem. Soc.* **2011**, *133* (4), 668−671.
(50) Schade, M.; Turner, C. J.; Kühne, R.; Schmieder, P.; Lowenhaupt, K.; Herbert, A.; Rich, A.; Oschkinat, H. The solution structure of the Zα domain of the human RNA editing enzyme ADAR1 reveals a prepositioned binding surface for Z-DNA. *Proc. Natl. Acad. Sci. U.S.A.* **1999**, *96* (22), 12465−12470.
(51) Rangadurai, A.; Szymaski, E. S.; Kimsey, I. J.; Shi, H.; Al-Hashimi, H. M. Characterizing micro-to-millisecond chemical exchange in nucleic acids using off-resonance R1ρ relaxation dispersion. *Prog. Nucl. Magn. Reson. Spectrosc.* **2019**, *112*−*113*, 55−102.
(52) Palmer, A. G., 3rd; Massi, F. Characterization of the dynamics of biomacromolecules using rotating-frame spin relaxation NMR spectroscopy. *Chem. Rev.* **2006**, *106* (5), 1700−1719.
(53) Palmer, A. G., III (2007). Chemical Exchange Effects in Biological Macromolecules. In *eMagRes.*; Harris, R. K.; Wasylishen, R. L., Eds., .
(54) Bothe, J. R.; Nikolova, E. N.; Eichhorn, C. D.; Chugh, J.; Hansen, A. L.; Al-Hashimi, H. M. Characterizing RNA dynamics at atomic resolution using solution-state NMR spectroscopy. *Nat. Methods* **2011**, *8* (11), 919−931.
(55) Mulder, F. A.; Mittermaier, A.; Hon, B.; Dahlquist, F. W.; Kay, L. E. Studying excited states of proteins by NMR spectroscopy. *Nat. Struct. Biol.* **2001**, *8* (11), 932−935.
(56) Lamers, M. M.; van den Hoogen, B. G.; Haagmans, B. L. ADAR1: "Editor-in-Chief" of Cytoplasmic Innate Immunity. *Front. Immunol.* **2019**, *10*, 1763.
(57) Herbert, A.; Schade, M.; Lowenhaupt, K.; Alfken, J.; Schwartz, T.; Shlyakhtenko, L. S.; Lyubchenko, Y. L.; Rich, A. The Zalpha domain from human ADAR1 binds to the Z-DNA conformer of many different sequences. *Nucleic Acids Res.* **1998**, *26* (15), 3486.
(58) Davis, P. W.; Hall, K.; Cruz, P.; Tinoco, I., Jr; Neilson, T. The tetraribonucleotide rCpGpCpG forms a left-handed Z-RNA double-helix. *Nucleic Acids Res.* **1986**, *14* (3), 1279−1291.
(59) Rich, A.; Nordheim, A.; Wang, A. H. The chemistry and biology of left-handed Z-DNA. *Annu. Rev. Biochem.* **1984**, *53*, 791−846.
(60) Rozners, E.; Moulder, J. Hydration of short DNA, RNA and 2'-OMe oligonucleotides determined by osmotic stressing. *Nucleic Acids Res.* **2004**, *32* (1), 248.
(61) Teng, M. K.; Liaw, Y. C.; van der Marel, G. A.; van Boom, J. H.; Wang, A. H. Effects of the O2' hydroxyl group on Z-DNA conformation: structure of Z-RNA and (araC)-[Z-DNA]. *Biochemistry* **1989**, *28* (12), 4923−4928.
(62) Foloppe, N.; MacKerell, A. D. Conformational Properties of the Deoxyribose and Ribose Moieties of Nucleic Acids: A Quantum Mechanical Study. *J. Phys. Chem. B* **1998**, *102* (34), 6669−6678.
(63) Egli, M.; Gessner, R. V. Stereoelectronic effects of deoxyribose O4' on DNA conformation. *Proc. Natl. Acad. Sci. U.S.A.* **1995**, *92* (1), 180−184.
(64) Mráziková, K.; Šponer, J.; Mlýnský, V.; Auffinger, P.; Kruse, H. Short-Range Imbalances in the AMBER Lennard-Jones Potential for (Deoxy)Ribose···Nucleobase Lone-Pair···π Contacts in Nucleic Acids. *J. Chem. Inf. Model.* **2021**, *61* (11), 5644−5657.
(65) Berger, I.; Egli, M.; Rich, A. Inter-strand C-H.O hydrogen bonds stabilizing four-stranded intercalated molecules: stereoelectronic effects of O4' in cytosine-rich DNA. *Proc. Natl. Acad. Sci. U.S.A.* **1996**, *93* (22), 12116−12121.
(66) Desiraju, G. R. The C-h···o hydrogen bond: structural implications and supramolecular design. *Acc. Chem. Res.* **1996**, *29* (9), 441−449.
(67) Behe, M.; Felsenfeld, G. Effects of methylation on a synthetic polynucleotide: the B−Z transition in poly(dG-m5dC).poly(dG-m5dC). *Proc. Natl. Acad. Sci. U.S.A.* **1981**, *78* (3), 1619−1623.
(68) Sugiyama, H.; Kawai, K.; Matsunaga, A.; Fujimoto, K.; Saito, I.; Robinson, H.; Wang, A. H. Synthesis, structure and thermodynamic properties of 8-methylguanine-containing oligonucleotides: Z-DNA under physiological salt conditions. *Nucleic Acids Res.* **1996**, *24* (7), 1272−1278.
(69) Balasubramaniyam, T.; Ishizuka, T.; Xiao, C. D.; Bao, H. L.; Xu, Y. 2'-O-Methyl-8-methylguanosine as a Z-Form RNA Stabilizer for Structural and Functional Study of Z-RNA. *Molecules* **2018**, *23* (10), 2572.
(70) Xu, Y.; Ikeda, R.; Sugiyama, H. 8-Methylguanosine: a powerful Z-DNA stabilizer. *J. Am. Chem. Soc.* **2003**, *125* (44), 13519−13524.
(71) Mittermaier, A. ZZ-Exchange. In *Encyclopedia of Biophysics*; Roberts, G. C. K., Ed.; Springer Berlin Heidelberg: Berlin, Heidelberg, 2013; pp 2796−2797..
(72) Palmer, A. G., 3rd Chemical exchange in biomacromolecules: past, present, and future. *J. Magn. Reson.* **2014**, *241*, 3−17.
(73) Shi, H.; Liu, B.; Nussbaumer, F.; Rangadurai, A.; Kreutz, C.; Al-Hashimi, H. M. NMR Chemical Exchange Measurements Reveal That N6-Methyladenosine Slows RNA Annealing. *J. Am. Chem. Soc.* **2019**, *141* (51), 19988−19993.
(74) Nardo, L.; Lamperti, M.; Salerno, D.; Cassina, V.; Missana, N.; Bondani, M.; Tempestini, A.; Mantegazza, F. Effects of non-CpG site methylation on DNA thermal stability: a fluorescence study. *Nucleic Acids Res.* **2015**, *43* (22), 10722−10733.
(75) Rausch, C.; Zhang, P.; Casas-Delucchi, C. S.; Daiß, J. L.; Engel, C.; Coster, G.; Hastert, F. D.; Weber, P.; Cardoso, M. C. Cytosine base modifications regulate DNA duplex stability and metabolism. *Nucleic Acids Res.* **2021**, *49* (22), 12870−12894.
(76) Rodríguez López, C. M.; Lloyd, A. J.; Leonard, K.; Wilkinson, M. J. Differential effect of three base modifications on DNA thermostability revealed by high resolution melting. *Anal. Chem.* **2012**, *84* (17), 7336−7342.
(77) Freier, S. M.; Kierzek, R.; Jaeger, J. A.; Sugimoto, N.; Caruthers, M. H.; Neilson, T.; Turner, D. H. Improved free-energy parameters for predictions of RNA duplex stability. *Proc. Natl. Acad. Sci. U.S.A.* **1986**, *83* (24), 9373−9377.
(78) Kypr, J.; Kejnovska, I.; Renciuk, D.; Vorlickova, M. Circular dichroism and conformational polymorphism of DNA. *Nucleic Acids Res.* **2009**, *37* (6), 1713−1725.

https://doi.org/10.1021/jacs.3c10406
J. Am. Chem. Soc. 2024, 146, 677−694

(79) Subramani, V. K.; Kim, K. K. Characterization of Z-DNA Using Circular Dichroism. *Methods Mol. Biol.* **2023**, *2651*, 33−51.
(80) Miyahara, T.; Nakatsuji, H.; Sugiyama, H. Helical structure and circular dichroism spectra of DNA: a theoretical study. *J. Phys. Chem. A* **2013**, *117* (1), 42−55.
(81) Nichols, P. J.; Bevers, S.; Henen, M. A.; Kieft, J. S.; Vicens, Q.; Vögeli, B. Adoption of A−Z Junctions in RNAs by Binding of Zα Domains. *Methods Mol. Biol.* **2023**, *2651*, 251−275.
(82) Chong, Y. E.; Guo, M.; Yang, X. L.; Kuhle, B.; Naganuma, M.; Sekine, S. I.; Yokoyama, S.; Schimmel, P. Distinct ways of G:U recognition by conserved tRNA binding motifs. *Proc. Natl. Acad. Sci. U.S.A.* **2018**, *115* (29), 7527−7532.
(83) Masquida, B.; Westhof, E. On the wobble GoU and related pairs. *RNA* **2000**, *6* (1), 9−15.
(84) Imhof, P.; Zahran, M. The effect of a G:T mispair on the dynamics of DNA. *PLoS One* **2013**, *8* (1), No. e53305.
(85) Patel, D. J.; Kozlowski, S. A.; Marky, L. A.; Rice, J. A.; Broka, C.; Dallas, J.; Itakura, K.; Breslauer, K. J. Structure, dynamics, and energetics of deoxyguanosine thymidine wobble base pair formation in the self-complementary d(CGTGAATTCGCG) duplex in solution. *Biochemistry* **1982**, *21* (3), 437−444.
(86) Ho, P. S.; Frederick, C. A.; Quigley, G. J.; van der Marel, G. A.; van Boom, J. H.; Wang, A. H.; Rich, A. G. G.T wobble base-pairing in Z-DNA at 1.0 A atomic resolution: the crystal structure of d(CGCGTG). *EMBO J.* **1985**, *4* (13A), 3617−3623.
(87) Ha, S. C.; Choi, J.; Hwang, H. Y.; Rich, A.; Kim, Y. G.; Kim, K. K. The structures of non-CG-repeat Z-DNAs co-crystallized with the Z-DNA-binding domain, hZα ADAR1. *Nucleic Acids Res.* **2009**, *37* (2), 629−637.
(88) Serra, M. J.; Smolter, P. E.; Westhof, E. Pronouced instability of tandem IU base pairs in RNA. *Nucleic Acids Res.* **2004**, *32* (5), 1824.
(89) Yu, Z.; Chen, T.; Cao, X. RNA editing by ADAR1 marks dsRNA as "self". *Cell Res.* **2015**, *25* (12), 1283−1284.
(90) Solomon, O.; Di Segni, A.; Cesarkas, K.; Porath, H. T.; Marcu-Malina, V.; Mizrahi, O.; Stern-Ginossar, N.; Kol, N.; Farage-Barhom, S.; Glick-Saar, E.; Lerenthal, Y.; Levanon, E. Y.; Amariglio, N.; Unger, R.; Goldstein, I.; Eyal, E.; Rechavi, G. RNA editing by ADAR1 leads to context-dependent transcriptome-wide changes in RNA secondary structure. *Nat. Commun.* **2017**, *8* (1), 1440.
(91) Braasch, D. A.; Corey, D. R. Locked nucleic acid (LNA): fine-tuning the recognition of DNA and RNA. *Chem. Biol.* **2001**, *8* (1), 1−7.
(92) Dumat, B.; Larsen, A. F.; Wilhelmsson, L. M. Studying Z-DNA and B- to Z-DNA transitions using a cytosine analogue FRET-pair. *Nucleic Acids Res.* **2016**, *44* (11), No. e101.
(93) Yi, J.; Yeou, S.; Lee, N. K. DNA Bending Force Facilitates Z-DNA Formation under Physiological Salt Conditions. *J. Am. Chem. Soc.* **2022**, *144* (29), 13137−13145.
(94) Herbert, A. To "Z" or not to "Z": Z-RNA, self-recognition, and the MDA5 helicase. *PLoS Genet.* **2021**, *17* (5), No. e1009513.
(95) Guo, X.; Liu, S.; Sheng, Y.; Zenati, M.; Billiar, T.; Herbert, A.; Wang, Q. ADAR1 Zα domain P195A mutation activates the MDA5-dependent RNA-sensing signaling pathway in brain without decreasing overall RNA editing. *Cell Rep.* **2023**, *42* (7), 112733.
(96) Mannion, N. M.; Greenwood, S. M.; Young, R.; Cox, S.; Brindle, J.; Read, D.; Nellåker, C.; Vesely, C.; Ponting, C. P.; McLaughlin, P. J.; Jantsch, M. F.; Dorin, J.; Adams, I. R.; Scadden, A. D.; Ohman, M.; Keegan, L. P.; O'Connell, M. A. The RNA-editing enzyme ADAR1 controls innate immune responses to RNA. *Cell Rep.* **2014**, *9* (4), 1482−1494.
(97) Lehmann, K. A.; Bass, B. L. The importance of internal loops within RNA substrates of ADAR1. *J. Mol. Biol.* **1999**, *291* (1), 1−13.
(98) Chung, H.; Calis, J. J. A.; Wu, X.; Sun, T.; Yu, Y.; Sarbanes, S. L.; Dao Thi, V. L.; Shilvock, A. R.; Hoffmann, H. H.; Rosenberg, B. R.; Rice, C. M. Human ADAR1 Prevents Endogenous RNA from Triggering Translational Shutdown. *Cell* **2018**, *172* (4), 811−824.e14.
(99) Wong, S. K.; Sato, S.; Lazinski, D. W. Elevated activity of the large form of ADAR1 in vivo: very efficient RNA editing occurs in the cytoplasm. *RNA* **2003**, *9* (5), 586−598.
(100) Pfaller, C. K.; Donohue, R. C.; Nersisyan, S.; Brodsky, L.; Cattaneo, R. Extensive editing of cellular and viral double-stranded RNA structures accounts for innate immunity suppression and the proviral activity of ADAR1p150. *PLoS Biol.* **2018**, *16* (11), No. e2006577.
(101) Koeris, M.; Funke, L.; Shrestha, J.; Rich, A.; Maas, S. Modulation of ADAR1 editing activity by Z-RNA in vitro. *Nucleic Acids Res.* **2005**, *33* (16), 5362.
(102) Chen, Y. G.; Hur, S. Cellular origins of dsRNA, their recognition and consequences. *Nat. Rev. Mol. Cell Biol.* **2022**, *23* (4), 286−301.
(103) Karki, R.; Sundaram, B.; Sharma, B. R.; Lee, S.; Malireddi, R. S.; Nguyen, L. N.; Christgen, S.; Zheng, M.; Wang, Y.; Samir, P.; Neale, G.; Vogel, P.; Kanneganti, T. D. ADAR1 restricts ZBP1-mediated immune response and PANoptosis to promote tumorigenesis. *Cell Rep.* **2021**, *37* (3), 109858.
(104) de Reuver, R.; Verdonck, S.; Dierick, E.; Nemegeer, J.; Hessmann, E.; Ahmad, S.; Jans, M.; Blancke, G.; Van Nieuwerburgh, F.; Botzki, A.; Vereecke, L.; van Loo, G.; Declercq, W.; Hur, S.; Vandenabeele, P.; Maelfait, J. ADAR1 prevents autoinflammation by suppressing spontaneous ZBP1 activation. *Nature* **2022**, *607* (7920), 784−789.
(105) Zhang, T.; Yin, C.; Fedorov, A.; Qiao, L.; Bao, H.; Beknazarov, N.; Wang, S.; Gautam, A.; Williams, R. M.; Crawford, J. C.; Peri, S.; Studitsky, V.; Beg, A. A.; Thomas, P. G.; Walkley, C.; Xu, Y.; Poptsova, M.; Herbert, A.; Balachandran, S. ADAR1 masks the cancer immunotherapeutic promise of ZBP1-driven necroptosis. *Nature* **2022**, *606* (7914), 594−602.
(106) Jiao, H.; Wachsmuth, L.; Kumari, S.; Schwarzer, R.; Lin, J.; Eren, R. O.; Fisher, A.; Lane, R.; Young, G. R.; Kassiotis, G.; Kaiser, W. J.; Pasparakis, M. Z-nucleic-acid sensing triggers ZBP1-dependent necroptosis and inflammation. *Nature* **2020**, *580* (7803), 391−395.
(107) Balachandran, S.; Mocarski, E. S. Viral Z-RNA triggers ZBP1-dependent cell death. *Curr. Opin. Virol.* **2021**, *51*, 134−140.
(108) Thapa, R. J.; Ingram, J. P.; Ragan, K. B.; Nogusa, S.; Boyd, D. F.; Benitez, A. A.; Sridharan, H.; Kosoff, R.; Shubina, M.; Landsteiner, V. J.; Andrake, M.; Vogel, P.; Sigal, L. J.; tenOever, B. R.; Thomas, P. G.; Upton, J. W.; Balachandran, S. DAI Senses Influenza A Virus Genomic RNA and Activates RIPK3-Dependent Cell Death. *Cell Host Microbe* **2016**, *20* (5), 674−681.
(109) Zhang, T.; Yin, C.; Boyd, D. F.; Quarato, G.; Ingram, J. P.; Shubina, M.; Ragan, K. B.; Ishizuka, T.; Crawford, J. C.; Tummers, B.; Rodriguez, D. A.; Xue, J.; Peri, S.; Kaiser, W. J.; López, C. B.; Xu, Y.; Upton, J. W.; Thomas, P. G.; Green, D. R.; Balachandran, S. Influenza Virus Z-RNAs Induce ZBP1-Mediated Necroptosis. *Cell* **2020**, *180* (6), 1115−1129.e13.
(110) Wittig, B.; Dorbic, T.; Rich, A. Transcription is associated with Z-DNA formation in metabolically active permeabilized mammalian cell nuclei. *Proc. Natl. Acad. Sci. U.S.A.* **1991**, *88* (6), 2259−2263.
(111) Monleón, D.; Esteve, V.; Celda, B. NMR study of hexanucleotide d(CCGCGG)2 containing two triplet repeats of fragile X syndrome. *Biochem. Biophys. Res. Commun.* **2003**, *303* (1), 81−90.
(112) Popenda, M.; Biala, E.; Milecki, J.; Adamiak, R. W. Solution structure of RNA duplexes containing alternating CG base pairs: NMR study of r(CGCGCG)2 and 2'-O-Me(CGCGCG)2 under low salt conditions. *Nucleic Acids Res.* **1997**, *25* (22), 4589.

NOTE ADDED AFTER ASAP PUBLICATION

This paper published ASAP on December 22, 2023 with errors in Table 4. The error was corrected and the paper reposted on December 22, 2023.

https://doi.org/10.1021/jacs.3c10406
J. Am. Chem. Soc. 2024, 146, 677−694